NASA / TM—1999-209050 AIAA–99–1864

Coupling of Low Speed Fan Stator Vane Unsteady Pressures to Duct Modes: Measured vs. Predicted

Daniel L. Sutliff
AYT Corporation, Brook Park, Ohio

Laurence J. Heidelberg and Edmane Envia
Glenn Research Center, Cleveland, Ohio

May 1999

The NASA STI Program Office . . . in Profile

Since its founding, NASA has been dedicated to the advancement of aeronautics and space science. The NASA Scientific and Technical Information (STI) Program Office plays a key part in helping NASA maintain this important role.

The NASA STI Program Office is operated by Langley Research Center, the Lead Center for NASA's scientific and technical information. The NASA STI Program Office provides access to the NASA STI Database, the largest collection of aeronautical and space science STI in the world. The Program Office is also NASA's institutional mechanism for disseminating the results of its research and development activities. These results are published by NASA in the NASA STI Report Series, which includes the following report types:

- TECHNICAL PUBLICATION. Reports of completed research or a major significant phase of research that present the results of NASA programs and include extensive data or theoretical analysis. Includes compilations of significant scientific and technical data and information deemed to be of continuing reference value. NASA's counterpart of peer-reviewed formal professional papers but has less stringent limitations on manuscript length and extent of graphic presentations.

- TECHNICAL MEMORANDUM. Scientific and technical findings that are preliminary or of specialized interest, e.g., quick release reports, working papers, and bibliographies that contain minimal annotation. Does not contain extensive analysis.

- CONTRACTOR REPORT. Scientific and technical findings by NASA-sponsored contractors and grantees.

- CONFERENCE PUBLICATION. Collected papers from scientific and technical conferences, symposia, seminars, or other meetings sponsored or cosponsored by NASA.

- SPECIAL PUBLICATION. Scientific, technical, or historical information from NASA programs, projects, and missions, often concerned with subjects having substantial public interest.

- TECHNICAL TRANSLATION. English-language translations of foreign scientific and technical material pertinent to NASA's mission.

Specialized services that complement the STI Program Office's diverse offerings include creating custom thesauri, building customized data bases, organizing and publishing research results . . . even providing videos.

For more information about the NASA STI Program Office, see the following:

- Access the NASA STI Program Home Page at ***http://www.sti.nasa.gov***

- E-mail your question via the Internet to help@sti.nasa.gov

- Fax your question to the NASA Access Help Desk at (301) 621-0134

- Telephone the NASA Access Help Desk at (301) 621-0390

- Write to:
  NASA Access Help Desk
  NASA Center for AeroSpace Information
  7121 Standard Drive
  Hanover, MD 21076

NASA / TM—1999-209050 AIAA–99–1864

Coupling of Low Speed Fan Stator Vane Unsteady Pressures to Duct Modes: Measured vs. Predicted

Daniel L. Sutliff
AYT Corporation, Brook Park, Ohio

Laurence J. Heidelberg and Edmane Envia
Glenn Research Center, Cleveland, Ohio

Prepared for the
5th Aeroacoustics Conference
sponsored by the American Institute of Aeronautics and Astronautics
and the Confederation of European Aerospace Societies
Seattle, Washington, May 10–12, 1999

National Aeronautics and
Space Administration

Glenn Research Center

May 1999

Available from

NASA Center for Aerospace Information
7121 Standard Drive
Hanover, MD 21076
Price Code: A03

National Technical Information Service
5285 Port Royal Road
Springfield, VA 22100
Price Code: A03

AIAA–99–1864

COUPLING OF LOW SPEED FAN STATOR VANE UNSTEADY PRESSURES TO DUCT MODES: MEASURED VS. PREDICTED

Daniel L. Sutliff*
AYT Corporation
Brook Park, Ohio 44142

Laurence J. Heidelberg* and Edmane Envia*
National Aeronautics and Space Administration
Glenn Research Center
Cleveland, Ohio 44135

Abstract

Uniform-flow annular-duct Green's functions are the essential elements of the classical acoustic analogy approach to the problem of computing the noise generated by rotor-stator interaction inside the fan duct. This paper investigates the accuracy of this class of Green's functions for predicting the duct noise levels when measured stator vane unsteady surface pressures are used as input to the theoretical formulation. The accuracy of the method is evaluated by comparing the predicted and measured acoustic power levels for the NASA 48" low speed Active Noise Control Fan. The unsteady surface pressures are measured by an array of microphones imbedded in the suction and pressure sides of a single vane, while the duct mode levels are measured using a rotating rake system installed in the inlet and exhaust sections of the fan duct. The predicted levels are computed using properly weighted integrals of measured surface pressure distribution. The data-theory comparisons are generally quite good particularly when the mode cut-off criterion is carefully interpreted. This suggests that, at least for low speed fans, the uniform-flow annular-duct Green's function theory can be reliably used for prediction of duct mode levels if the cascade surface pressure distribution is accurately known.

Introduction

The periodic interaction of fan viscous wakes with stator vanes is a principal source of tone noise in modern turbofan engines. This source, referred to as rotor-stator interaction noise, occurs at discrete tones corresponding to the blade passing frequency (BPF) and its harmonics. Rotor-stator interaction noise can have a significant impact on the noise exposure problem during takeoff and landing. In view of the stringent community noise regulations and the noise reduction goals of NASA's Advanced Subsonic Technology program, it is highly desirable to have a method for accurate prediction of this source.

The most commonly used method for predicting rotor-stator interaction noise has been a version of Lighthill's acoustic analogy that employs uniform-flow annular-duct Green's functions. These functions are used to establish a connection between the unsteady surface pressure distribution on the stator vanes and the duct mode levels[1]. Prior work[2] has shown that for low to moderate tip speed fans, such a methodology produces quite reasonable qualitative data-theory agreement, but tends to fall short when it comes to detailed quantitative comparisons. Clearly, the shortcoming is caused by either inaccurate prediction of unsteady surface pressure distribution or the inadequacy of the uniform-flow Green's function representation (or perhaps both).

For the most part, prediction of the unsteady surface pressure distribution on a stator vane is accomplished via the so-called strip theory which accounts for the variations of the unsteady response along the airfoil span only parametrically, but is otherwise a 2D model of the inherently 3D unsteady aerodynamic response. Compounding the problem is the fact that the typical 2D cascade response models use zero thickness flat plates to represent the airfoil section geometry. Genuinely 3D unsteady aerodynamic models which account for both three-dimensionality of unsteady response and the blade geometry are not yet rigorously tested or widely available. Therefore, a detailed assessment of the impact of the unsteady aerodynamic response on the accuracy of the rotor-stator noise prediction models remains an open question.

* Senior Member, AIAA.

On the other hand, if 3D unsteady response was available through other means, the reliability of the Green's function approach could be investigated. To that end, the 3D unsteady vane surface pressure distribution for a representative fan was experimentally measured. This involved developing a technique for reliably measuring the time-dependent surface pressures with sufficient resolution in both space and time to allow for the construction of an accurate "picture" of unsteady blade response. In conjunction with such measurements, the duct noise levels were also measured to allow for a comparison between the predicted duct mode levels based on the measured unsteady response and measured duct mode levels.

To reduce the technical complexity of the measurements to a manageable level, the low-speed Active Noise Control Fan[3,4] (ANCF) facility located at the NASA Glenn Research Center was chosen as the test bed. The ANCF has a 16-bladed variable-pitch rotor and can be configured with stator vanes to generate a specific duct mode mix for aeroacoustic research. A unique feature of the ANCF rig is the direct attachment of the rotor centerbody to the rig support column thus eliminating the need for support struts that tend to introduce extraneous sources. The combination of the low tip speed (~400 ft/sec) and the 48" diameter produces interaction tones that are in the same frequency range as those of a full-size modern turbofan. A schematic of the ANCF is shown in figure 1.

The unsteady surface pressures were measured on the suction and pressure sides of a single stator vanes using imbedded miniature microphones. The harmonic magnitude and phase information from these microphones were used as input to the theoretical duct noise model to predict mode power levels (PWL) for comparison with measured PWL obtained via a rotating rake system.

The rotating rake system is an implementation of an idea originally conceived by T.G. Sofrin[5] and developed at NASA Glenn[6] whereby a rake with radially distributed pressure transducers rotates circumferentially in the direction of the fan at a precise fraction of the fan rotational speed. Since each circumferential acoustic mode rotates at a unique speed in the rotor frame of reference, a known Doppler shift occurs for that mode in the rake frame of reference allowing for separation of the circumferential mode content of the measured acoustic pressure field. Further decomposition of each circumferential mode into its radial mode content is accomplished via a least-squares curve fit using the Bessel basis functions.

Experimental Measurements

Fan Characteristics

The feature of the ANCF rig that makes it a unique tool for code validation is its flexibility. Choosing the proper stator vane count will result in particular mode combinations that can be studied in isolation. For this study 13-, 14-, 26-, and 28-vane counts were configured. Thus, the effect of generating a single mode, or two radial modes for a single circumferential mode, or two circumferential modes, each with a single radial mode, can be studied independently. The chord is the same for all vane configurations, so the solidity varies with the vane count in contrast to the classical fixed solidity studies.

The modes generated by rotor-stator interaction, and their nominal cut-off RPM, at the rotor station (hub-to-tip radius ratio of 0.31) are shown in Table I. Fan speeds from 1000 to 1900 corrected RPM were run with an emphasis on speeds where new modes cut-on.

The fan rotor blade has an average chord length of 4.5". The stator vane chord is a constant 4.5". Nominal rotor-stator spacing is measured at the hub from the fan trailing edge to the stator leading edge which, for this experiment, was set at half the vane chord.

Duct Mode Data

The in-duct mode PWL was measured at the same corrected fan speeds as were run for the vane pressure data. The rake/vane data were taken within a few hours of one another. The rotating rake was installed such that the mode levels are measured very near the inlet entrance or exhaust exit release plane. The modal pressure coefficients are converted to mode PWL assuming all the power is flowing in one direction. This implies that there is no significant termination reflection or standing waves. This assumption has been shown to be valid for the inlet[7], but is less accurate for the exhaust propagation.

Vane Instrumentation

A single vane was instrumented on both the suction and pressure sides with miniature microphones. 60 microphones (30 on each side) were installed. The vane was split on the mean camber line to allow installation and replacement of the microphones. The microphone locations for the corresponding suction/pressure pair were chosen to be nominally the same chord and span locations.

A small offset in the span direction was required to physically accommodate the microphone pairs. The nominal locations are shown in figure 2. Three main chord lines were instrumented as well as a single span line at the 20% chord location. For the 14-vane configuration, a pair of instrumented vanes was used to add a span line at the 85% chord location. One vane had eight microphones on the suction side while the other had eight at the corresponding locations on the pressure side. Thus, the unsteady pressures were measured at a total of 76 locations (for the 14 vane configuration only). The microphone locations were obtained by the intersection point of the surface normal with the mean camber line as illustrated in figure 3.

The unsteady pressure time histories were synchronously sampled at 256 samples-per-revolution for 1250 fan revolutions and recorded via a digital acquisition system. A time domain average with an ensemble length of one fan revolution was performed to further extract the tone signal. An FFT was performed on the suction and pressure side time-domain averaged histories from which the BPF and 2BPF-magnitude and phase information was extracted.

Vane Surface Pressure Data

Figures 4 through 7 present the unsteady surface pressures for the 14-vane configuration at 1800 corrected RPM. The magnitude and phase of the unsteady surface pressures were extracted at frequencies corresponding to BPF and 2BPF for the suction and pressure sides separately. In this paper, the magnitudes are presented as sound pressure levels (SPL). The unsteady pressure levels for other RPM and vane configurations are included in the appendix.

Figure 4 shows the unsteady surface pressure levels at BPF along the three main chord lines at 49%, 74%, and 91% span locations. On both sides of the vane, the SPL shows the expected higher levels near the leading edge although the trend is less dramatic on the pressure side. On the suction side of the vane, an unexpected increase in the levels was noted near the trailing edge at the 91% and 74% span locations where flat-plate analyses would suggest rapidly decreasing levels. At the 74% span location, chord pressures show minimums near 25% and 70% chord stations. The levels on the pressure side show a maximum near the leading edge and decaying amplitude along the chord. A less severe rise at the trailing edge is also evident here. The phase of the unsteady pressure on both sides is fairly constant indicating a long wavenumber gust.

To help identify the spanwise trends, the BPF data along two span lines, at 20% chord and 85% chord, are presented in figure 5. The suction side shows an approximately linear advance in phase from the hub to the tip indicating that the wake impacts on the hub first. This is consistent with the wake lean noted in the hotwire measurements taken on the ANCF earlier[2]. On the pressure side, there is a rapid change in phase near the tip region an indicator, perhaps, of a complex tip flow.

The 2BPF magnitude and phase chordwise distributions are shown in figure 6. In general, these levels are 10 dB below the BPF levels. On the suction side, there are two chordwise phase cycles at 91% span, one at the 74% span location, and none at 49%. The pressure side shows little indication of phase cycles. The chordwise phase cycles on the suction side are qualitatively consistent with the classical view of the gust-airfoil interactions, but perhaps less so on the pressure side. Figure 7 shows the corresponding spanwise plots. At the 20% chord location, there are no cycles in the spanwise phase, while there is at least one cycle evident at 85% chord location. Of course, the lack of sufficient resolution at the 2BPF makes wave form interpretation somewhat subjective. The corresponding data for the other vane configurations are presented in the appendix.

To help identify the relationship between the measured vane pressures and duct acoustic levels, the following metric was introduced:

$$p_l = \frac{S_v}{10^{-12}\rho_o a_o}\left\{\frac{1}{3}\left[\sum^{41\%,74\%,94\%}\left(\overline{\Delta P_{rms}}\right)\right]^2\right\} \qquad (1)$$

Here P_{rms} denotes the average unsteady chordwise pressure, Δ indicates the difference (i.e., suction side minus pressure side) and the overbar the chordwise sum of measured pressures. The nominal medium impedance is given by $\rho_o a_o$ and the quantity 10^{-12} is the reference acoustic power (in Watts). Somewhat arbitrarily, the area, S_v, was chosen as the surface area of a single vane. It should be emphasized that p_l is defined only to give a rough estimate of the "average power" radiated by the vane unsteady surface pressures absent multi-vane, near-field, or duct boundary effects. Phase was ignored in the computation of the averaging loading since it was relatively uniform, particularly at BPF.

Variations of the metric p_l as a function of fan RPM for all vane counts are shown in figure 8. At BPF, the results show monotonic increases with RPM, except for the 13-vane configuration, which shows a local rise near 1400. This is related to the cut on of the mode (3,0) at 1392 RPM. Doubling the vane count increases p_l by a couple of dB at BPF. At 2BPF, the metric for the 14- and 28-vane configurations shows monotonic increases with RPM with the 28 vane at a slightly higher level. For 13- and 26-vane configurations it shows a significant rise near 1750 RPM.

Next, in figure 9, a comparison of the power metric and tone PWL obtained from the rotating rake measurements is shown. In general, the trends in p_l are very similar to those of tone mode PWL. In particular, the steep increase in tone PWL centered near 1750 RPM for the 26-vane configuration is matched by an equally dramatic increase in the vane power value. This increase in duct mode level had been noted in an earlier study[8]. The reason for the dramatic increase is unknown but thought to be related to some resonance-like condition in the unsteady pressures. An examination of the results for 26 vanes in the appendix shows that the phase response of the unsteady pressures is relatively flat at 2BPF near 1750 RPM when compared to the 28-vane case. Overall, the similarity of the trends in figure 9 is most probably due to the particular geometry of the ANCF and the modest variations of the chordwise phase of the unsteady pressures at all vane counts.

Theoretical Model

Duct Mode Description

The theoretical framework for describing the modal structure of the rotor-stator interaction noise using uniform-flow Green's function is well established and, therefore, need only be outlined here. However, where necessary, improvements made to the standard model will be pointed out.

The acoustic analogy based formula for the harmonic acoustic pressure field generated inside a hard-walled, annular duct, containing a uniform mean flow is given by[9]:

$$p'(\vec{x};\omega) = \int_S \nabla G(\vec{x} \mid \vec{x}_s;\omega)\cdot \hat{n}_s f(\vec{x}_s;\omega) d\vec{x}_s \qquad (2a)$$

$$\vec{x} = (x, r, \theta), \quad \vec{x}_s = (x_s, r_s, \theta_s) \qquad (2b)$$

where G is the Green's function, f the unsteady loading distribution on the vanes and $\hat{n}_s$ the unit surface normal. $\vec{x}$ is an arbitrary field point inside the duct and $\vec{x}_s$ an arbitrary source location on the vanes. ω, the harmonic tone frequency, is equal to $jN_B\Omega$ where Ω is the rotational speed of the fan, N_B the fan blade count and j the tone harmonic index. The integration is to be carried out over the surface of the vane cascade denoted by S. The requirement that the boundary condition on the duct walls is satisfied leads to a representation of G in terms of the eigenmodes of the annular duct. The result is:

$$G(\vec{x}/\vec{x}_s;\omega) = \sum_m \sum_n \frac{1}{\sqrt{1-\frac{1}{\xi_{mn}^2}}} \times \Psi_{mn}(r,\theta)\Psi_{mn}^*(r_s,\theta_s) \qquad (3a)$$

$$\Psi_{mn}(r,\theta) = \left[AJ_m(\kappa_{mn}r) + BY_m(\kappa_{mn}r)\right] \qquad (3b)$$

$$k_{mn}^{\pm} = \frac{k}{\beta_0^2}\left(-M_0 \pm \sqrt{1-\frac{1}{\xi_{mn}^2}}\right) \qquad (3c)$$

$$k = \frac{\omega}{a_0}, \qquad \beta_0 = \sqrt{1-M_0^2}, \qquad \xi_{mn} = \frac{k}{\beta_0\kappa_{mn}} \qquad (3d)$$

where M_o and a_o are the Mach number and speed of sound of the medium inside the duct. Ψ_{mn}'s represent the normal modes (i.e., eigenfunctions) of the duct indexed by m, the circumferential mode order, and n, the radial mode order. J_m and Y_m are Bessel functions of the first and second kind, respectively. κ_{mn}'s denote the radial eigenvalues for the duct. $k_{mn}^{\pm}$ is the axial wavenumber with the minus sign denoting the upstream moving acoustic wave and plus sign the downstream moving acoustic wave. ξ_{mn}, the cut-off ratio of the mode, determines which modes propagate for a given frequency, Mach number and hub-to-tip radius ratio. Modes for which ξ_{mn} is greater than unity propagate, otherwise they are cut-off (i.e., evanescent).

Once the unsteady pressure distribution f is known over the vane surfaces, Eq. (2a) can be used to compute the acoustic pressure field in the duct which, in view of the modal nature of G, can also be represented in a modal form. In essence, the sound field inside the duct is envisaged as being caused by an unsteady source distribution on the vane cascade. The unsteady source distribution (i.e., f) is induced by the rotor unsteady wake upwash.

In the usual application of these formulae two simplification are made. First, the vanes are assumed to be twisted, zero thickness, flat plates. Second, the strip approximation is invoked to model the unsteady vane loading at each radius independently of the rest of the span. This greatly facilitates the task of computing the surface integral in Eq. (2a). In this simplified approach, both the vane geometry and the unsteady loading distribution depend parametrically on the radius (i.e., r), but are otherwise two-dimensional functions of x and θ only.

Despite its obvious computational advantage, such a simplification ignores several potentially significant features of the loading distribution on a real vane. For example, while for a true 3D loading distribution the boundary condition on the vane is satisfied simultaneously everywhere on the cascade surface, each 2D strip loading distribution satisfies the boundary condition only at its own local radius, but violates it elsewhere on the vane surface. This has the effect of introducing additional sources where none exist. In addition, the orientation of the local chordwise lift vector for a real airfoil section typically varies from the leading edge to the trailing edge. This variation can exert a significant additional influence on the "split" of the acoustic field in the upstream and downstream direction beyond the mere orientation of the whole section (i.e., the stagger angle effect). Finally, aerodynamically speaking, in the case of a real blade row, the non-uniform mean flow tends to distort the incoming gust (i.e., wake) causing differences in amplitude and the phase of the upwash experienced by the two sides of the vane. This, in turn, causes differences between the resulting unsteady pressure distributions on the two sides of the vane. This effect is totally absent from the flat-plate cascade response theories because they use a "frozen gust" model of the incident wake.

Measured unsteady pressure distributions are by their very nature 3D and include all of the real flow effects discussed above. As a result the surface integration in Eq. (2a) is somewhat more complicated as it must account for the airfoil geometry and local surface orientation. The unit normal $\hat{n}_s$ can then be expressed in terms of the gradient of the surface profile. Substituting in Eq. (2a) yields

$$p'(\vec{x}) = \int_s Q(\vec{x}|\vec{x}_s) f(\vec{x}_s) \mathrm{d}\vec{x}_s \tag{4a}$$

$$Q(\vec{x}|\vec{x}_s) = \frac{1}{|\nabla S|} \times \left(\frac{\partial G}{\partial x_s}\frac{\partial S}{\partial x_s} + \frac{\partial G}{\partial r_s}\frac{\partial S}{\partial r_s} + \frac{1}{r_s}\frac{\partial G}{\partial \theta_s}\frac{\partial S}{\partial \theta_s} \right) \tag{4b}$$

where the dependence on the frequency parameter ω is implied in Eqs. (4a and 4b) but is omitted for the sake of brevity. In general, all the terms in the integrand depend on the surface coordinates (x_s, r_s, θ_s). In a strip approximation, the radial derivatives in Eq. (4b) are neglected and the remaining terms reduce to simple forms[10]. It should be emphasized that the integral is the sum of contributions from both the pressure side and suction side of vane.

In general, the integral in Eq. (4a) is too complex to compute in closed form and must be integrated by a quadrature scheme. This can be done, for example, by dividing the surface into small "panels" whose individual contributions to the integral can be computed analytically. The number of panels can always be chosen so as to ensure a desired accuracy in the calculations. Naturally, given that the measured vane unsteady pressure distributions presented earlier are relatively sparse, it is necessary to interpolate them over the vane surface for high-resolution computation of the surface integrals.

Interpolation of Unsteady Pressure Distributions

Recall the surface microphone layout in figure 2 and typical measured chordwise and spanwise distributions of amplitude and phase of unsteady vane surface pressures shown in figures 4 and 5. While, from a purely mathematical point of view, there are many ways to interpolate the measured pressures over the surface, the nature of the aerodynamic interaction places restrictions on the allowable form of interpolation. For example, note that the measured spanwise phase at 20% chord location shows an essentially monotonic variation, and that the chordwise phase distributions at the three spanwise locations 49%, 74%, and 91% are generally very similar. This observation suggests that when interpolating the pressures one should ensure a similar behavior for the interpolated phases. Similar arguments could be invoked for the amplitude interpolation.

Beyond the nature of the interpolation scheme to use, one is also faced with the question of which quantities to interpolate. Specifically, should the phase and amplitude be interpolated, or is it preferable to interpolate the real and imaginary parts of the pressure? Although both strategies were examined, the focus was on the amplitude and phase method. The choice was motivated by the notion that phase variation is more or less monotonic along both the chordwise direction (from the leading to the trailing edge), and the spanwise direction (from hub to tip) thus lending itself more easily to simple interpolation schemes. For the sake of completeness however, comparisons of the acoustic results generated by both methods will be presented.

The particular interpolation scheme utilized in this paper employs a two-tiered approach whereby a coarse distribution of the chosen quantity is produced first and is later used to generate distributions of any desired resolution. The coarse distribution is obtained over a coarse grid that has the same chordwise and spanwise spacing as the microphone location layout but covers the entire vane surface. Using the spanwise data at the 20% chord location as the "anchor" points, the chordwise distributions where no data was taken were filled in by interpolating in between the main chord lines at the 49%, 74%, and 91% span locations. In constructing the interpolating function, which is done separately for the region between the 49% and 74% locations, and the region between the 74% and 91% locations, the known boundary data are weighted in linear proportions to their proximity to the point under consideration. Therefore, the missing chord lines are filled in by linearly blending chordwise profiles of the known data anchored to the 20% chord locations along the span. Then, the Kutta condition is enforced along the trailing edge by stipulating zero surface pressure difference everywhere along the span. When completed, this method produces interpolated values in a "box" bounded between the 49% and 91% span locations, and between the 20% and 100% chord locations. Next, extrapolations are performed to cover the rest of the surface. This begins by using the first two chord locations at each spanwise station to form a linear extrapolating function, which is then evaluated at the leading edge to obtain an estimate of the unsteady pressures (i.e., amplitude and phase) there. Similar procedures involving quadratic and cubic schemes produce virtually identical acoustic results despite the differences in the values of the extrapolated leading edge surface pressures. Finally, employing a linear extrapolation scheme along the spanwise direction, the missing locations between the hub (i.e., 31% span) and 49% span, and between the 91% span and the tip (i.e., 100% span) are filled to complete the matrix. At this point coarse distributions of both the amplitude and phase have been constructed. An identical procedure can be used should one choose to use the real and imaginary parts of the measured unsteady surface pressures instead. It should be emphasized that the interpolation is carried out on the pressure values themselves not on their corresponding SPL values shown in figures 4 through 7. In particular, the interpolation was performed on the amplitude in linear units and on the phase in degrees.

With a coarse distribution of the interpolated unsteady pressure data now available, the quadrature-based surface integration defined by Eqs. (4a and 4b) can be computed. Of course, since typically one will use a more resolved surface grid than that defined by the coarse grid, a second stage interpolation would be needed, but that would involve only interpolations and no extrapolations.

Once the acoustic pressure is computed, the time averaged acoustic power generated inside the duct due to rotor-stator interaction can be calculated. The expression for acoustic power, appropriate to a uniformly moving-medium, is given by:

$$p = \int_{A_D} \left[\left(1 + M_0^2\right) \langle \acute{p}\, \acute{u}^* \rangle + \frac{M_0}{\rho_0 a_0} \langle \acute{p}\, \acute{p}^* \rangle + \rho_0 a_0 M_0 \langle \acute{u}\acute{u}^* \rangle \right] dA \qquad (5)$$

where u' is the acoustic particle velocity and A_D the cross-sectional area of the duct. The symbol $\langle \bullet \rangle$ denotes time averaging over one period $2\pi/\omega$. Once, p' is known, u' can easily be calculated via the momentum equation. After some algebra , on a per mode basis, the power is given by:

$$p_{mn} = \frac{M_0 \beta_0^4 \sqrt{1 - \frac{1}{\xi_{mn}^2}}}{\left(1 \pm M_0 \sqrt{1 - \frac{1}{\xi_{mn}^2}}\right)^2} \acute{p}_{mn} \acute{p}^*_{mn} \qquad (6)$$

where p' is mode pressure and the symbol * denotes complex conjugate. Duct mode power level predictions based on Eq. (6) are the principal quantities that are used in comparisons with the measurements presented in the next section.

DISCUSSION

Effect of Analytical Model Implementation on PWL Predictions

Since the theory presented in this paper models the acoustics of an infinite constant-area duct, it does not account for duct area change effects. Therefore, the comparisons are carried out on the basis of acoustic power which accounts for area change.

The theoretical power levels were computed for BPF and 2BPF tones (when cut-on) for all vane configurations and fan RPM considered in this study. The calculations were carried out on a mode-by-mode basis and the resulting modal powers were summed to provide the total power in each tone at each fan speed. Both upstream and downstream acoustic power levels were computed.

The power calculations, however, proved problematic when computing the variation of mode power near cut-on (i.e., when $\xi_{mn} = 1$). The problem arises because, in the immediate neighborhood of cut-on, the Green's function is nearly singular due to the presence of the term $\sqrt{1-\frac{1}{\xi_{mn}^2}}$ in the denominator (see Eq. (3a)). The mode power level (see Eq. (6)), therefore, also exhibits that same singularity in the denominator. In theory, this singularity is offset by the vanishing of numerator terms in the integrand of Eq. (4a) so as to provide a finite mode power level. In practice, however, this offset would not occur unless the unsteady pressure distribution is known with sufficient accuracy in the vicinity of mode cut-on point. Since, in this work, the measured unsteady distributions used in the mode level calculations result from interpolating originally sparse distributions, some error is inevitably introduced in the computations of the numerator terms near cut-on. The end result of this is an exaggerated mode power level near $\xi_{mn} = 1$. The effect can be quite dramatic with predicted power levels exceeding by an order of magnitude, or more, the measured levels near the cut-on point. It should be pointed out, the same difficulty would occur with predicted unsteady surface pressures if, for whatever reason, they were not known accurately.

To circumvent this problem it was necessary to "soften" the mode cut-on criterion somewhat by avoiding the immediate neighborhood of the cut-on point. This was accomplished by stipulating that a mode is considered cut-on when $\xi_{mn} \geq 1+\varepsilon$ where ε is a small positive number. To ensure consistency, ε must depend on the tone harmonic order, because the cut-on criterion depends on the tone harmonic order and, hence, any errors incurred at BPF will be doubled at 2BPF, tripled at 3BPF and so forth. Therefore, in this paper, the soft criterion was defined as $\xi_{mn} \geq 1+0.03j$ where j is the tone harmonic order. The specific choice of the numerical value was determined by a careful examination of the predicted mode levels for all vane counts and RPM.

The impact of the modified criterion on the predicted levels is summarized in figure 10 where both hard and soft cut-on criteria results are compared against the measured power levels. For the sake of brevity, the comparison is carried out on a total (i.e., upstream + downstream) radiated power basis for each tone. Clearly, when a mode just cuts-on (see Table I), the hard criterion produces significant over-predictions compared with the data. The soft criterion, on the other hand, generates levels that are in much better agreement with the measurements. The difference between the two criteria is particularly dramatic for the 28-vanes configuration where the hard cut-on levels are some 15 dB above the measured ones when a mode just cuts-on. In contrast, the corresponding soft cut-on levels follow very closely the data. In view of the significant improvement in data-theory comparisons, in the remainder of the paper only results based on the soft cut-on criterion will be presented. Further discussion of these results and their analysis on a mode-by-mode basis will be given later in section.

To revisit the issue of interpolating the amplitude and phase of surface pressure as opposed to interpolating its real and imaginary parts, figure 11 illustrates the comparison of the two methods on the total power basis. While quantitatively the two schemes produce similar results, qualitatively the predictions based on the amplitude and phase tend to produce better data-theory agreement, especially as at 2BPF where it is expected that phase variation is more critical. Therefore, from here on only results based on the amplitude and phase interpolation will be discussed.

Therefore the basis on which the analytical predictions are presented in the next section is interpolation on amplitude and phase, and soft cut-on condition ($\xi_{mn} \geq 1+0.03j$).

Comparison of Analytical Predictions to Experimental Measurements of Mode PWL

The comparison of the Green's function analytical predictions to the levels measured by the rotating rake is presented in figures 12 through 14. The basis of comparison is the duct mode power levels of the cut-on rotor-stator interaction modes. It should be noted that the analytical solution predicts the levels at the source and does not include rotor reflection and transmission effects, area change reflections, or duct termination; i.e. the mode is generated and propagates in an infinite duct. The rotating rake measurements are taken very near the inlet entrance or exhaust exit planes which are at different hub-to-tip radius ratios (figure 1).

The total mode power level, the sum of all modes fore and aft, is presented at BPF and 2BPF in figure 12 for all vane counts. The agreement between theory and data is generally excellent. The difference at BPF is less than 1-2 dB with minor exceptions. At 2BPF, the agreement is very good. The differences are greater at a some speeds most likely due to the relatively lower spatial resolution at the smaller wavelength at 2BPF. The 26-vane configuration is an exception to the general agreement. The trend is correct but the analytical solution over predicts the PWL by approximately 6 dB. The 26-vane case is interesting due to the very sharp increase in mode PWL over a narrow

RPM range. It is thought to be due to a resonance like condition in the unsteady aerodynamic response of the stator vane. The reader is invited to compare the magnitude and phase trends for the 26- and 28- vane configurations shown in the appendix as this is beyond the scope of this paper. A follow-up paper using this data will investigate the aerodynamic response for this specific case as well as the general cases.

The data-theory comparison of the inlet and exhaust mode PWL are presented for 13 and 14 vanes in figure 13a at BPF and 2BPF; 26 and 28 vanes in figure 13b for 2BPF. The analytical solution tends to over predict the inlet PWL while under predicting the exhaust PWL at BPF. This discrepancy may be due to rotor reflection/transmission effects. The 26-vane configuration at 2BPF generates the (6,0) mode only so the total is a result of a single mode. The inlet prediction matches levels to within a few dB. The previously noted disagreement in total PWL levels for the 26-vane configuration can be seen to arise primarily from an over prediction in the exhaust (6,0) mode level. The prediction for the 28-vane configuration matches very well except in the exhaust near cut-on of the (4,1) radial (1522 RPM). The comparisons at 2BPF are very good but show some of the scatter about the measured levels, again probably due to lower effective resolution.

The separation into individual circumferential and radial modes in the inlet and exhaust ducts is presented in figure 14. Multiple rotor-stator interaction modes exist only at 2BPF at the RPM investigated. The 13-vane configuration shown on figure 14a generates two circumferential modes, each with a single radial. The agreement is very good except at 1600 RPM in the inlet. The 14-vane configuration generates a single m-order with two radials as shown in figure 14b. The analytical prediction is very good. The levels are scattered about the measured values generally within 5 dB. The 28-vane configuration also generates the (4,0) and (4,1). This comparison is presented on figure 14c. The comparisons in the inlet are very good, but in the exhaust are less favorable.

Conclusion

The unsteady surface pressures were measured on the suction and pressure sides of a single stator vane installed on the NASA Glenn 48" Active Noise Control Fan. A uniform-flow annular-duct Green's function model was developed to predict the duct mode PWL based on the experimentally acquired surface pressures. The model accounts for real airfoil geometry. These predictions were compared to the duct mode PWL measured by the rotating rake measurement system.

The results of this paper indicate that the uniform-flow annular-duct Green's function method accurately predicts the duct mode PWL given the unsteady pressure distribution, except very near cut-off. Modifying the cut-off condition improves the data-theory comparisons significantly. The theory accurately predicts the total PWL at BPF, although inlet levels are over predicted, while the exhaust levels are under predicted. This may indicate a physical mechanism beyond the investigative scope of this paper, possibly rotor reflection/transmissions. At 2BPF, the total levels, as well as the inlet/exhaust levels are accurately predicted; though the scatter about the data is slightly greater due to lower resolution at the higher frequency. The individual mode PWL are predicted reasonably well.

A follow-up study using the unsteady aerodynamic data from this paper to investigate the ability of current methods to accurately predict the unsteady response of a cascade is planned.

Appendix

The vane pressure data is presented in an appendix following the figures. The magnitude and phase delta between the suction and pressure side is presented for brevity. Data for BPF and 2BPF are shown for the 13-, 14-, 26-, and 28-vane configurations in figures A1 to A16. These data may be used for validation of analytical and numerical studies.

References

[1]Goldstein, M.E., *Aeroacoustics*, McGraw-Hill, New York, 1976.

[2]Sutliff, D.L., Bridges, J.E., and Envia, E., "Comparison of Predicted Low Speed Fan Rotor/Stator Interaction Modes to Measured," AIAA Paper 97–1609, May 1997.

[3]Heidelberg, L.H., Hall, D.G., Bridges, J.E., and Nallasamy, M., "A Unique Ducted Fan Test Bed for Active Noise Control and Aeroacoustic Research," NASA TM–107213, May 1996, AIAA Paper 96–1740, May 1996.

[4]Sutliff, D.L., Nallasamy, M., Heidelberg, L.J., and Elliott, D.M., "Baseline Acoustic Levels of the NASA Active Noise Control Fan Rig," NASA TM–107214, May 1996, AIAA Paper 96–1745, May 1996.

[5]Pickett, G.F., Sofrin, T.G., and Wells, R.A., "Method of Fan Sound Mode Structure Determination. Final Report," NASA CR–135293, August 1977.

[6]Heidelberg, L. and Hall, D.G., "Inlet Acoustic Mode Measurements Using a Continuously Rotating Rake," AIAA Journal of Aircraft, July–August 1996, pp. 761–767.

[7]Nallasamy, M., Sutliff, D.L., and Heidelberg, L.J., "Propagation of Spinning Acoustic Modes in Turbofan Exhaust Modes," AIAA Paper 99–0481, January 1999.

[8]Sutliff, D.L., "ANCF Research," Proceedings of the AST Engine Noise Workshop, Session 4: Fan Noise Experiments," pp. 277–294, April 21–23, 1998.

[9]Envia, E., Huff, D.L., and Morrison, C.R., "Analytical Assessment of Stator Sweep and Lean in Reducing Rotor-Stator Tone Noise," AIAA Paper 96–1791, May 1996.

[10]Meyer, H.D. and Envia, E., "Aeroacoustic Analysis of Turbofan Noise Generation," NASA CR–4715, pp. 29, Eq. 4.31, 1996.

TABLE I.—ROTOR-STATOR INTERACTION MODES (M,N) CUT-OFF RPM

[At the three relevant hub-to-tip ratios, σ]

(a) At the Inlet Plane (σ = 0.0)

	Harmonic	
Vane count	BPF	2BPF
13	(3,0) @ 1398	(6,0) @ 1249 (-7,0) @ 1422
14	(2,0) @ 1017	(4,0) @ 886 (4,1) @ 1546
26	– – – – – – –	(6,0) @ 1249
28	– – – – – – –	(4,0) @ 886 (4,1) @ 1546

(b) At the Stator Plane (σ = 0.31)

	Harmonic	
Vane count	BPF	2BPF
13	(3,0) @ 1392	(6,0) @ 1250 (-7,0) @ 1430
14	(2,0) @ 987	(4,0) @ 885 (4,1) @ 1522
26	– – – – – – –	(6,0) @ 1250
28	– – – – – – –	(4,0) @ 885 (4,1) @ 1522

(c) At the Exit Plane (σ = 0.5)

	Harmonic	
Vane count	BPF	2BPF
13	(3,0) @ 1316	(6,0) @ 1248 (-7,0) @ 1422
14	(2,0) @ 894	(4,0) @ 862 (4,1) @ 1468
26	– – – – – – –	(6,0) @ 1248
28	– – – – – – –	(4,0) @ 862 (4,1) @ 1468

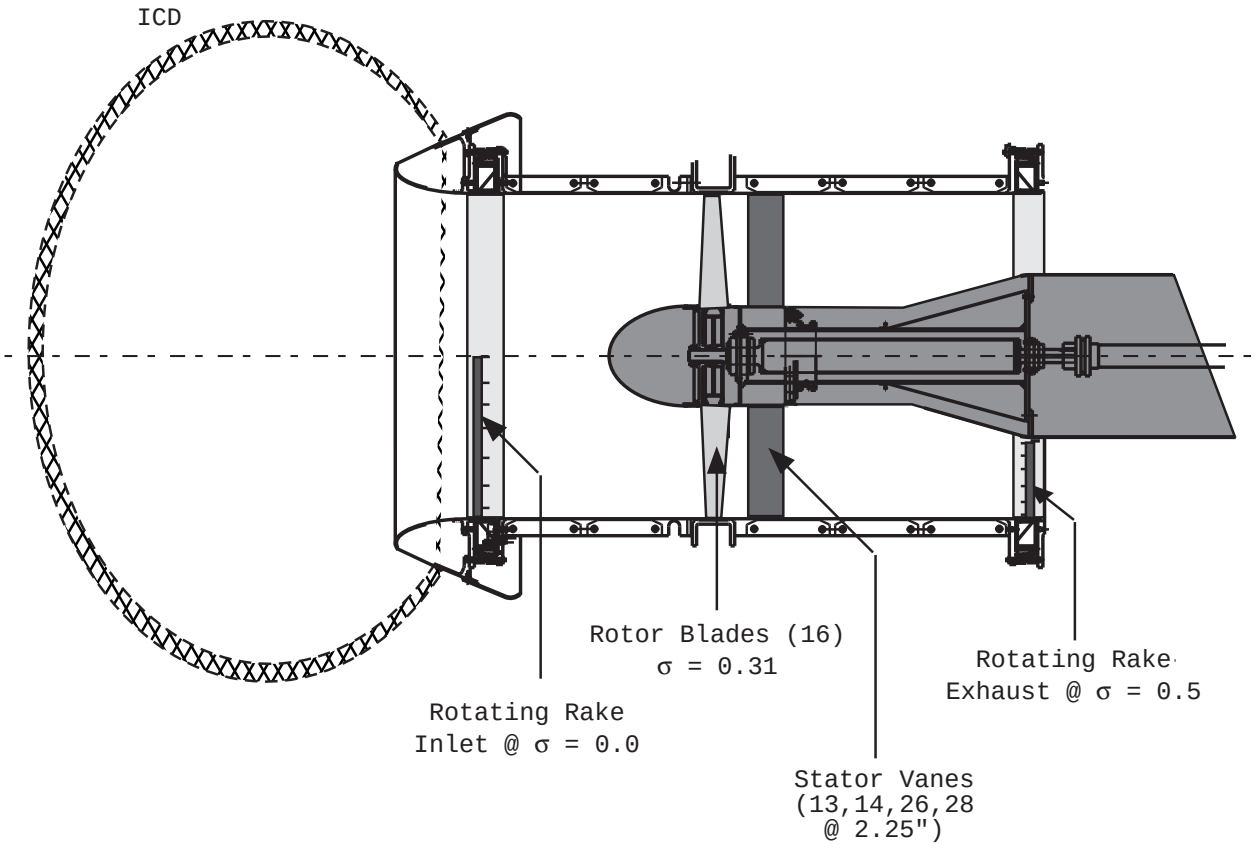

Figure 1.—Schematic of Active Noise Control Fan Rig.

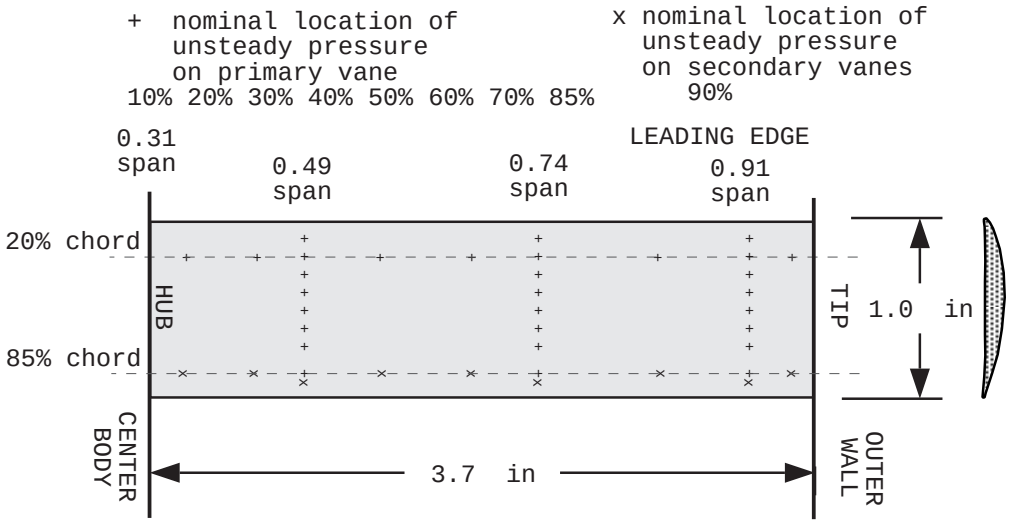

Figure 2.—ANCF Instrumented Stator Vane Pressure Measurement Locations.

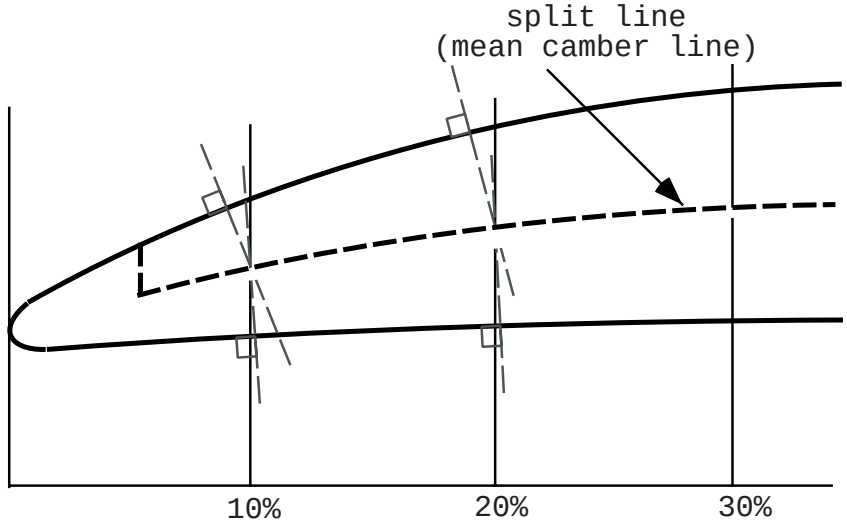

Figure 3.—Chord Definition for Stator Vane Pressure Measurement Locations.

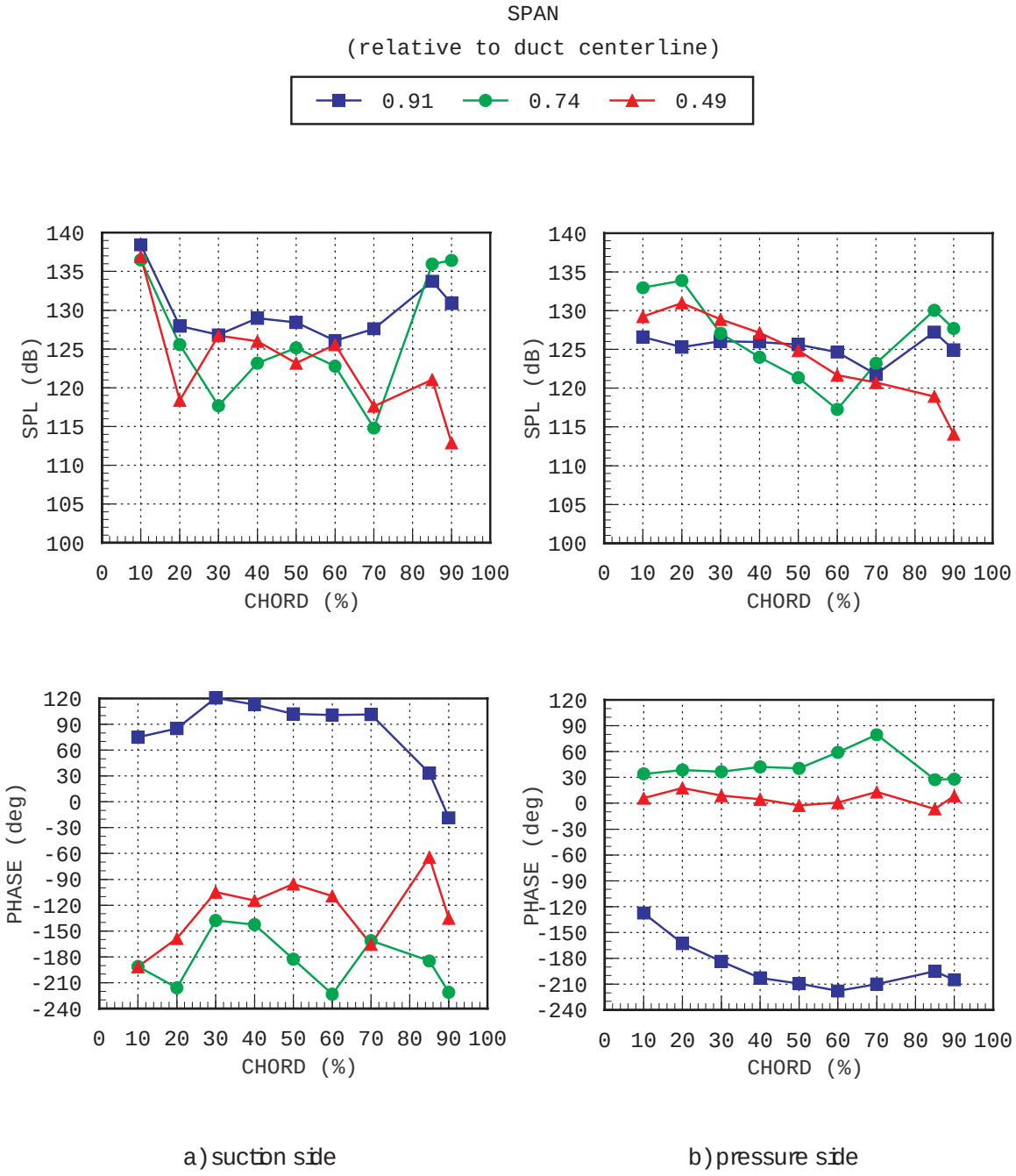

Figure 4.–ANCF Stator Vane Unsteady Pressures Variation along Chord Line.
(14 Vanes * RPM = 1800 * BPF)

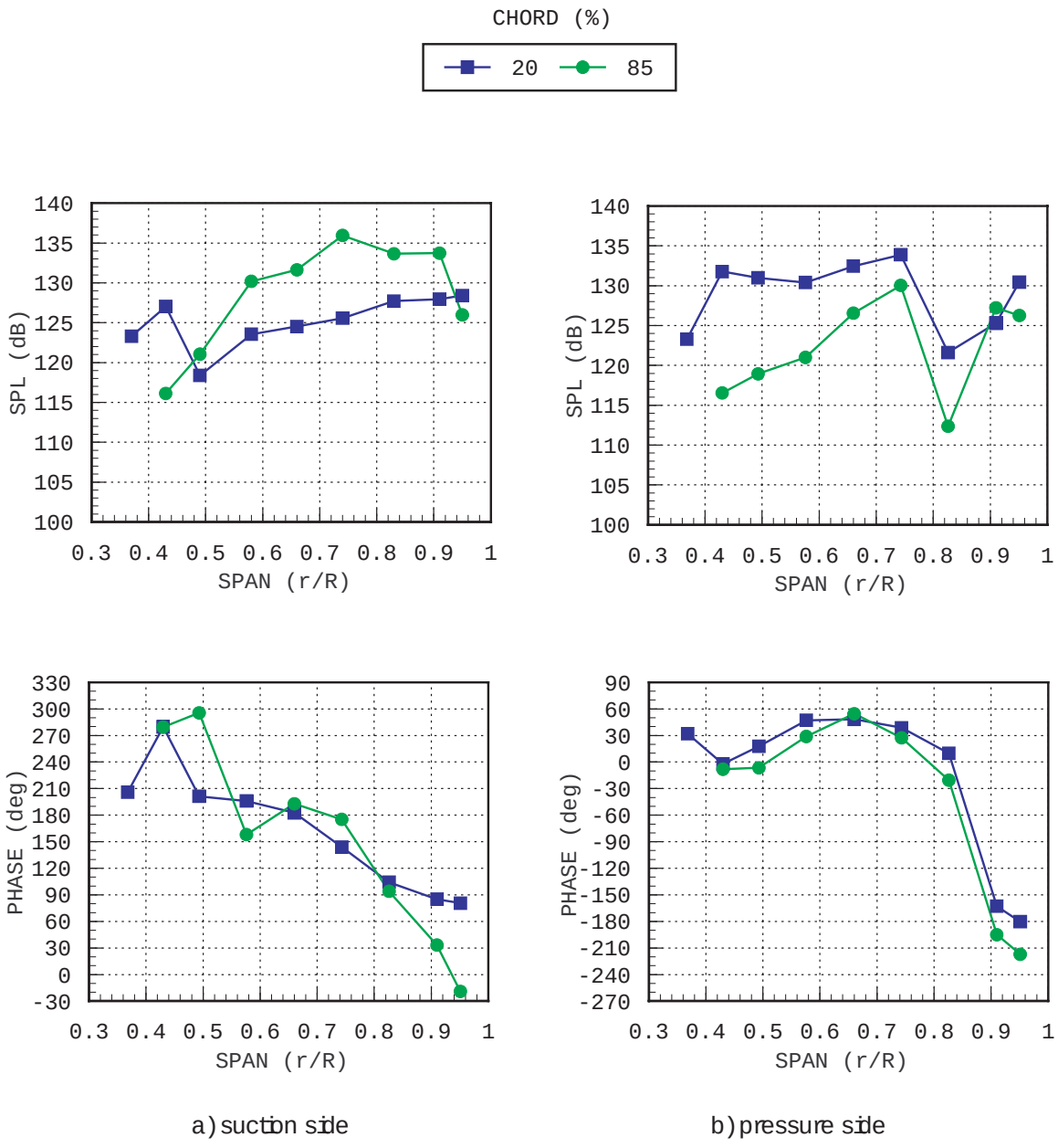

Figure 5.–ANCF Stator Vane Unsteady Pressures Variation along Span Line.
(14 Vanes * RPM = 1800 * BPF)

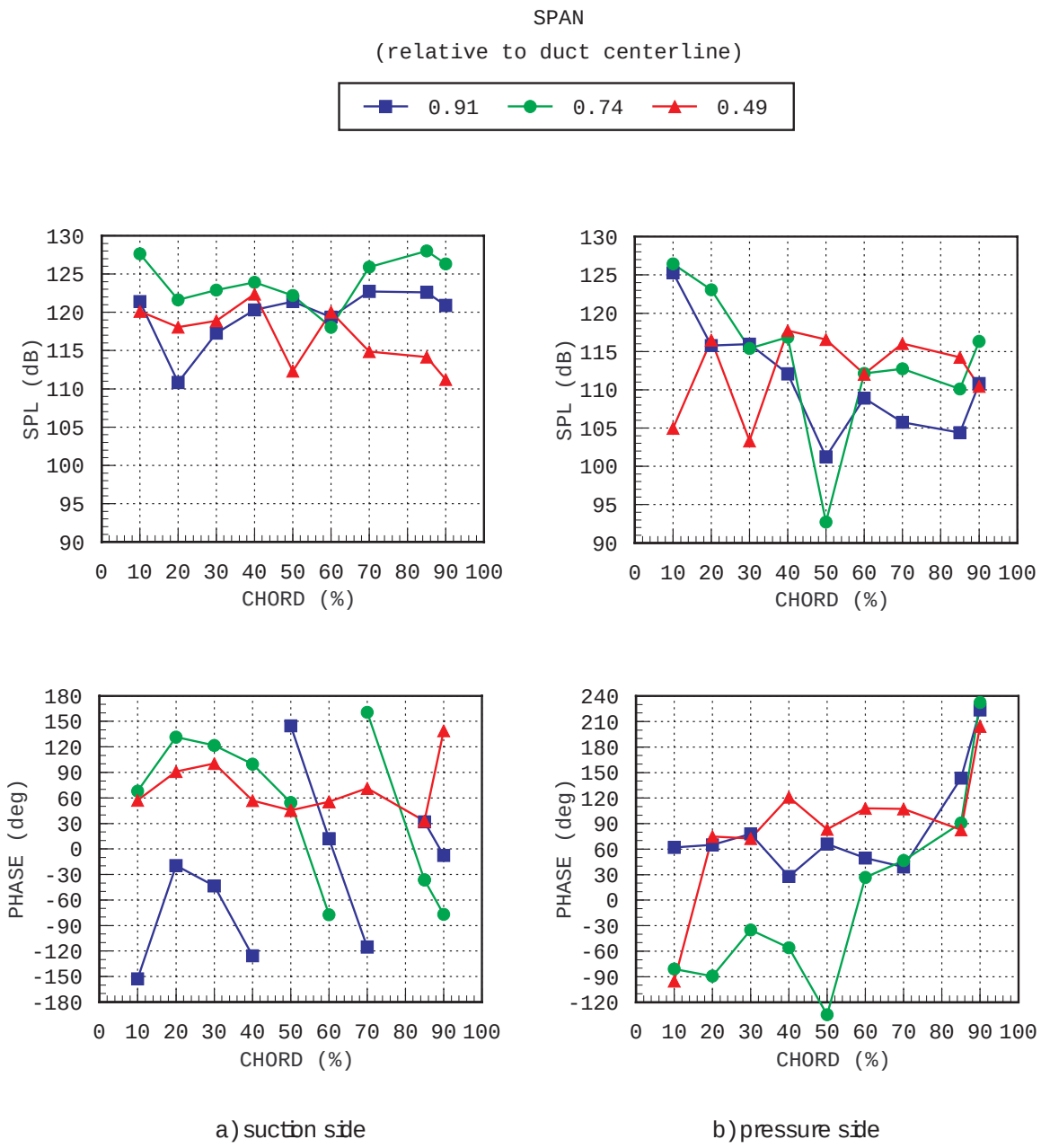

Figure 6.–ANCF Stator Vane Unsteady Pressures Variation along Chord Line.
(14 Vanes * RPM = 1800 * 2BPF)

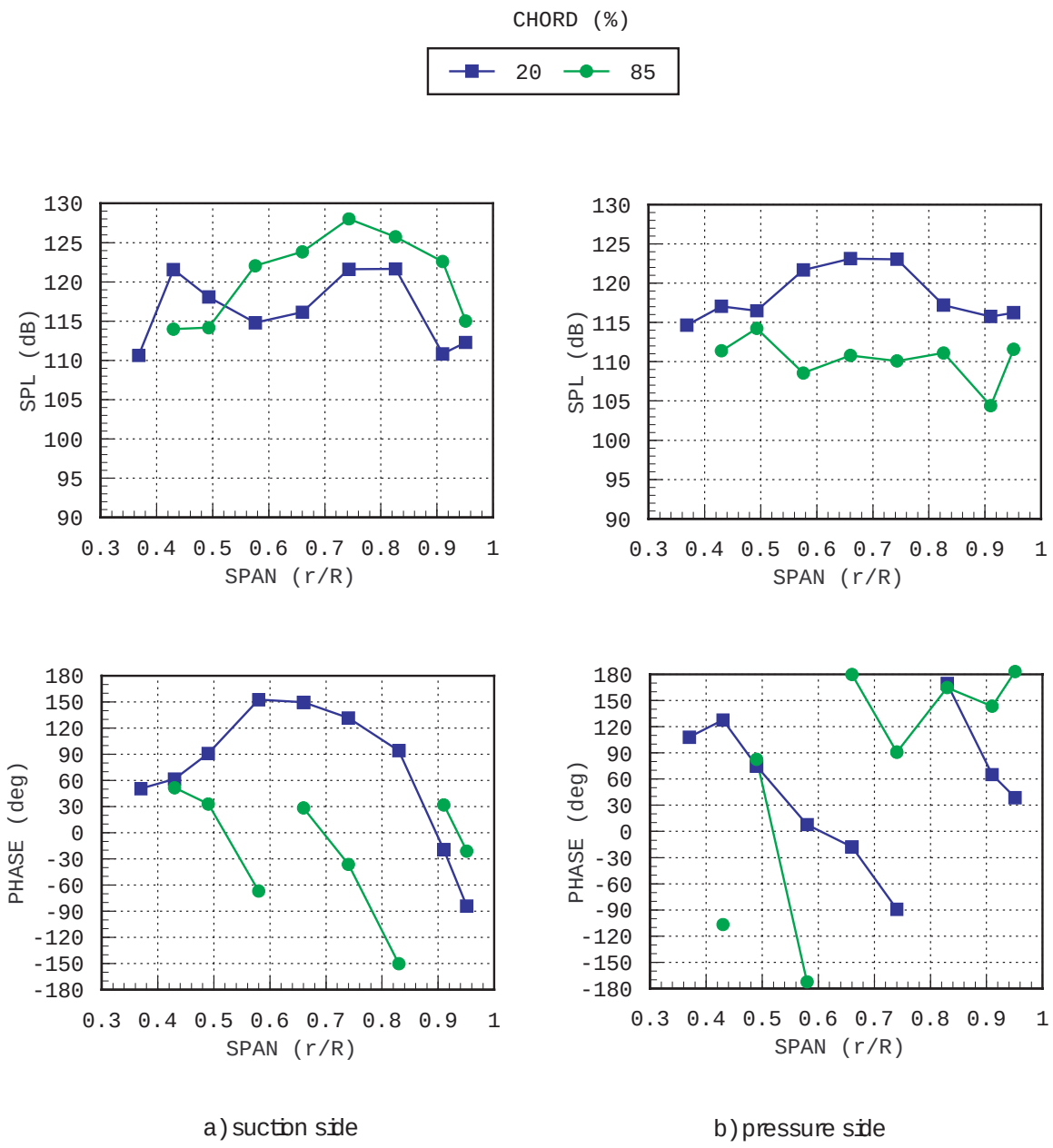

a) suction side

b) pressure side

Figure 7.–ANCF Stator Vane Unsteady Pressures Variation along Span Line.
(14 Vanes * RPM = 1800 * 2BPF)

$$p_l = \frac{S_v}{10^{-12}\rho_o a_o}\left\{\frac{1}{3}\left[\sum^{41\%,74\%,94\%}\left(\overline{\Delta P_{rms}}\right)\right]^2\right\} \quad (1)$$

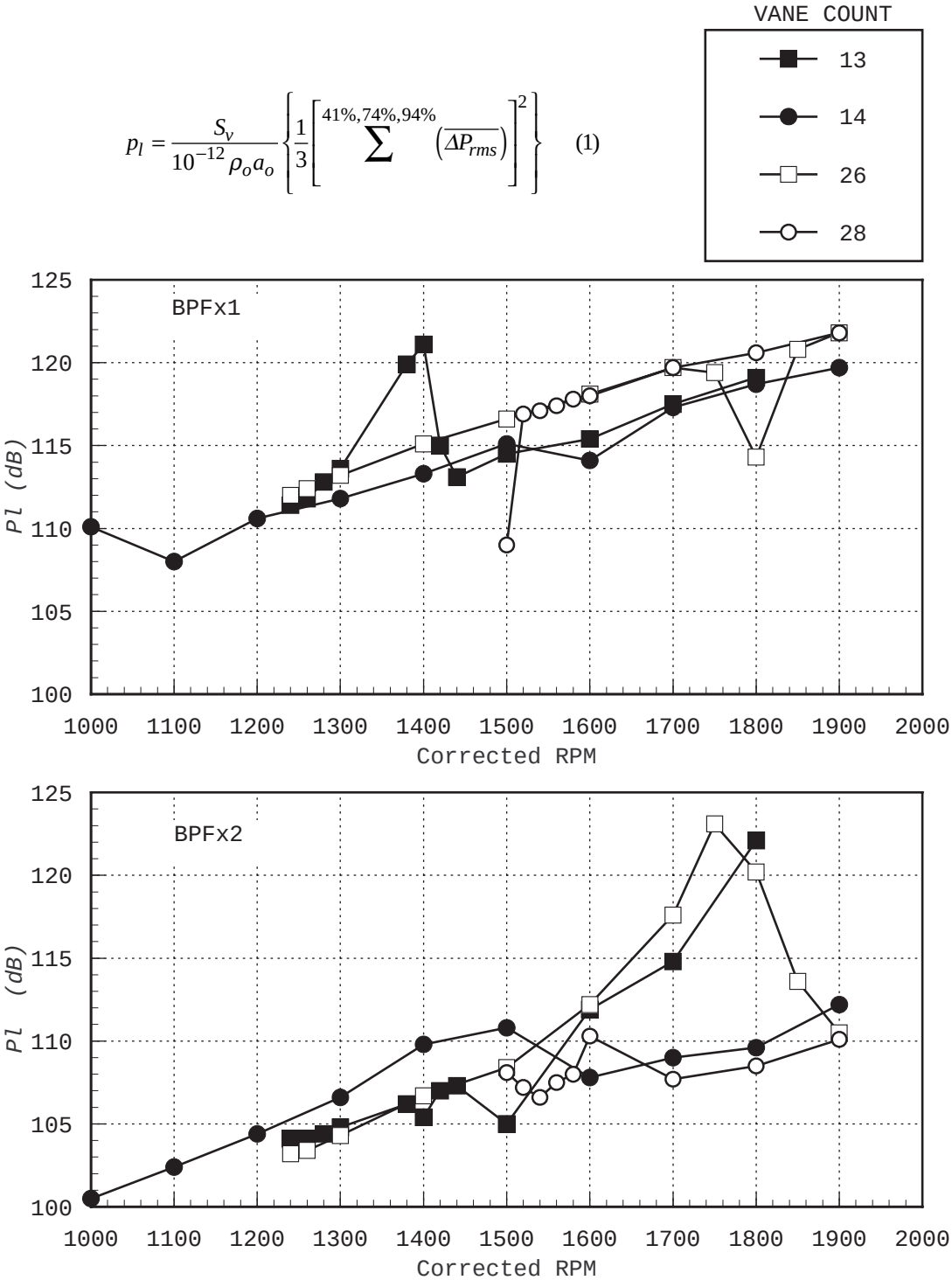

Figure-8. Estimated Single Vane Average "Power".

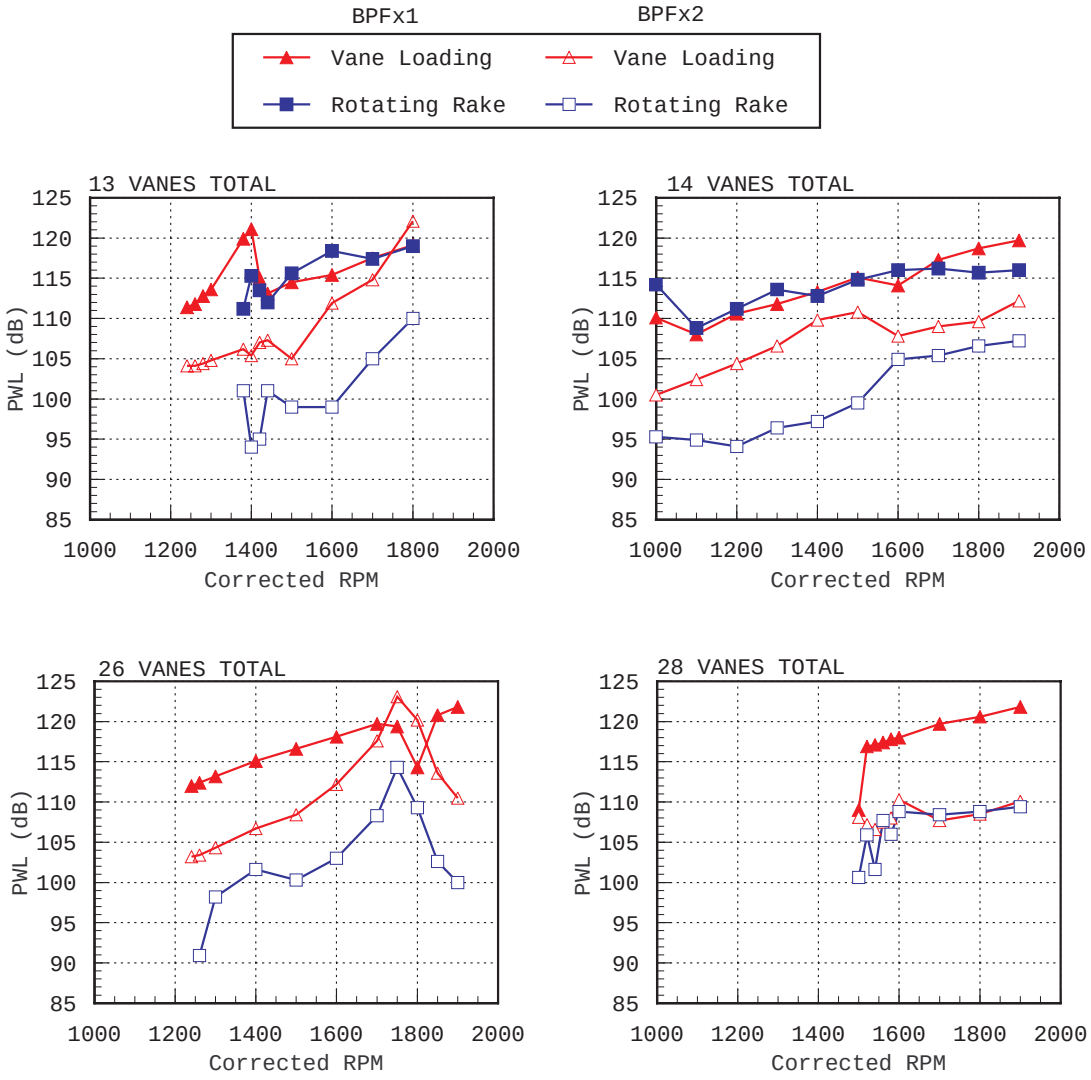

Figure 9.– Comparison of Integrated Stator Vane Pressures to Mode PWL.
(Total PWL at BPF & 2BPF)

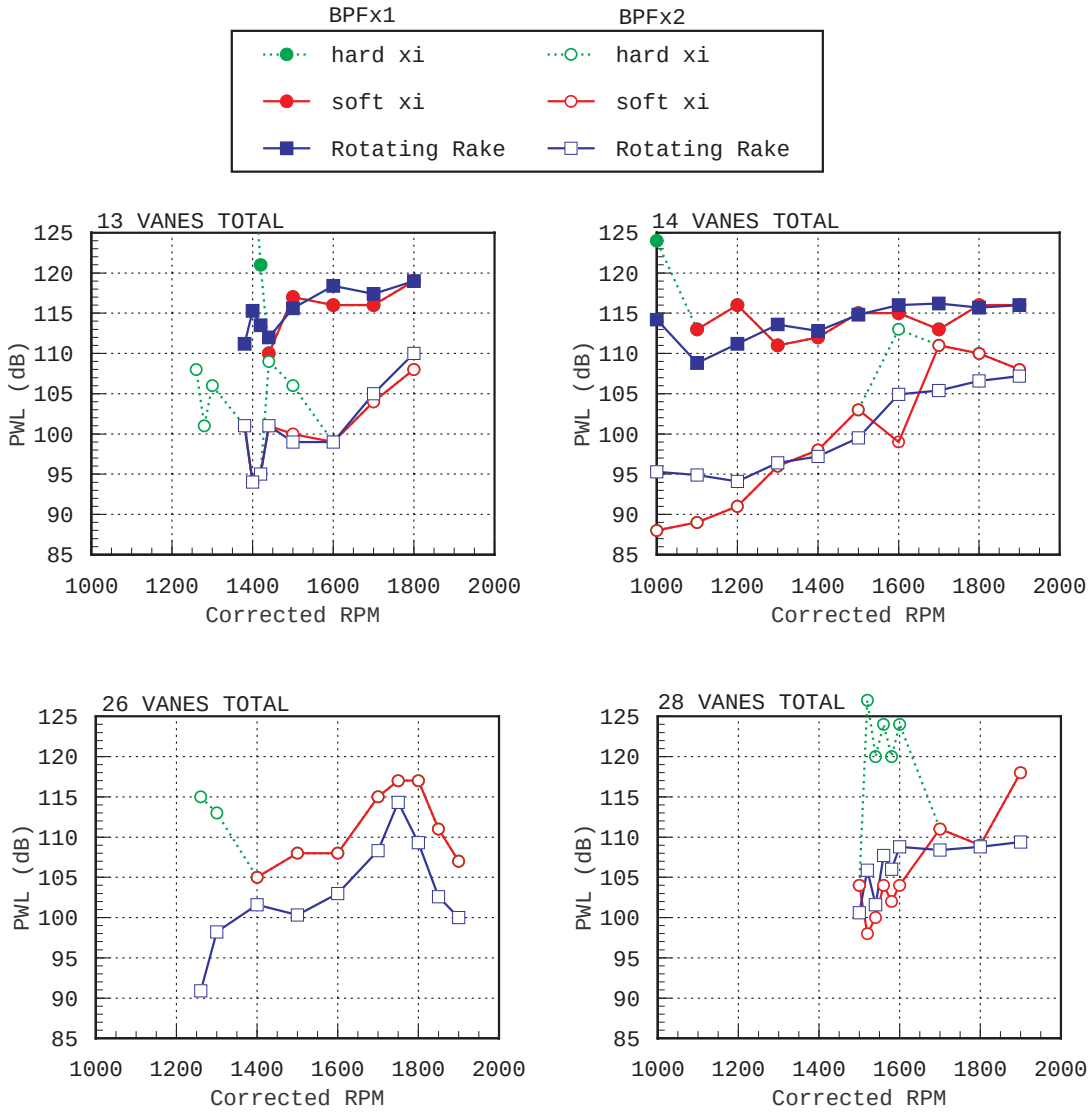

Figure 10.–Analytical Comparison of Cut-off Ratio Boundary.

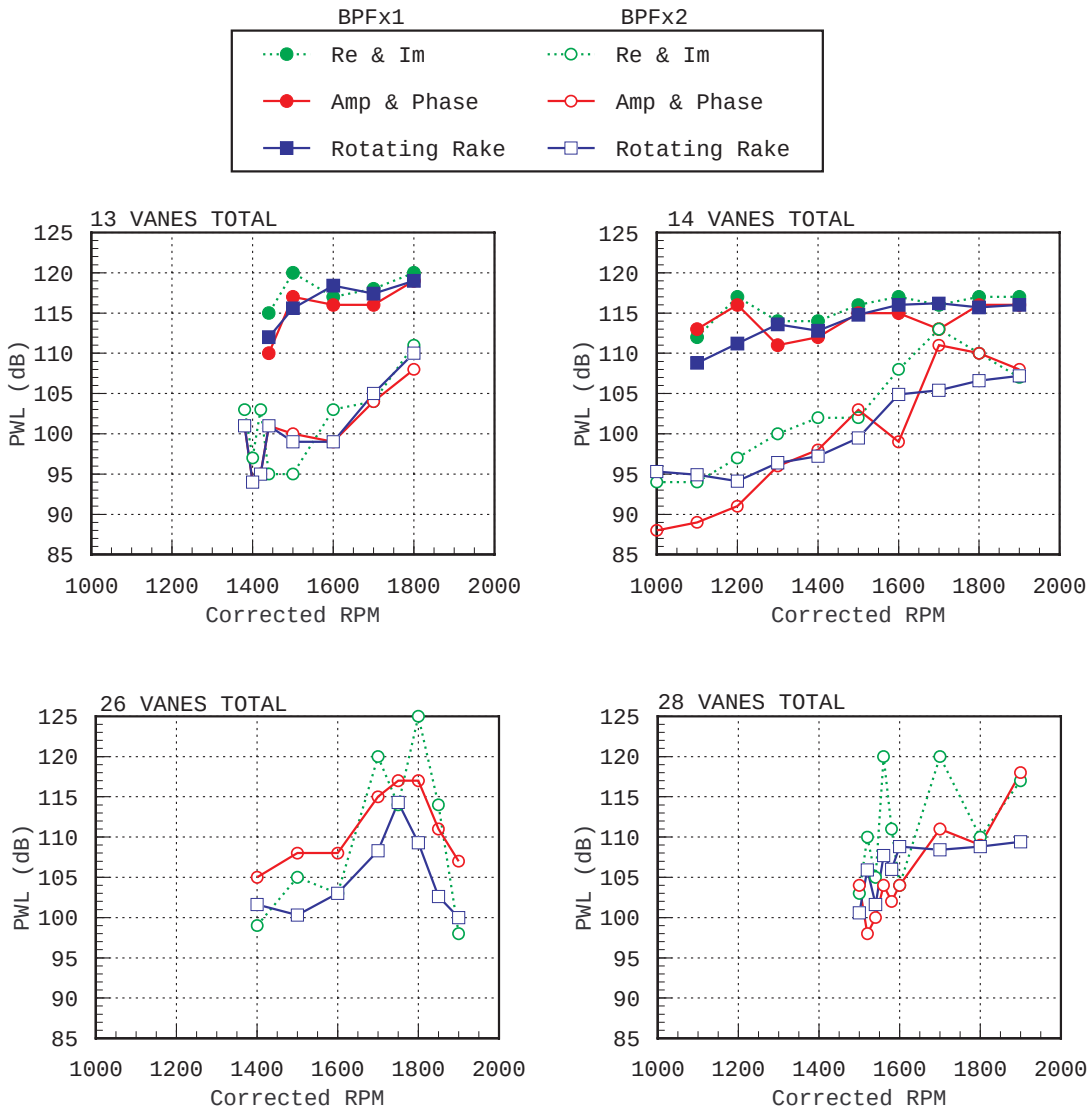

Figure 11.–Analytical Comparison of Interpolation Methods.

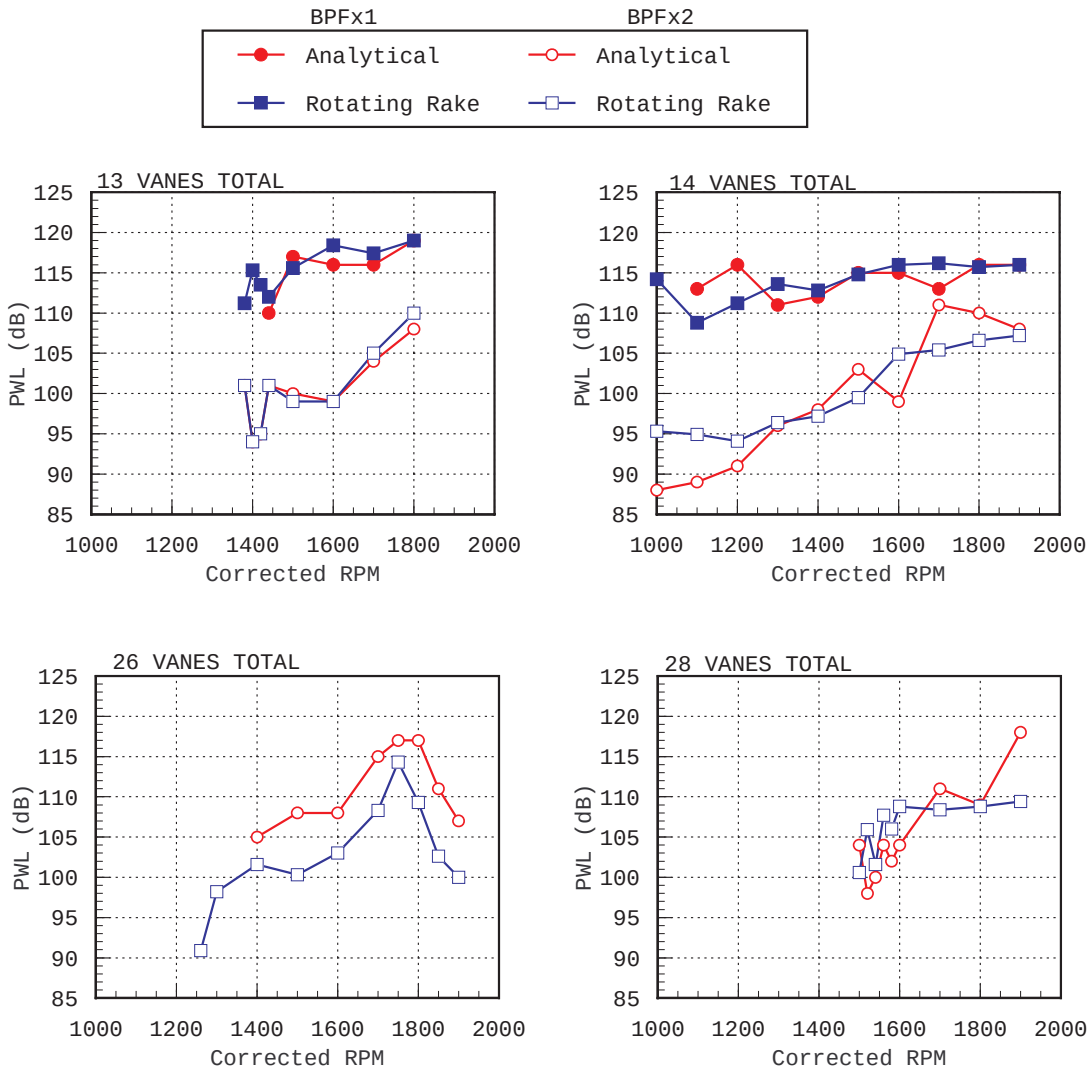

Figure 12.–Comparison of Analytical to Measured Mode PWL.
(Total PWL at BPF & 2BPF)

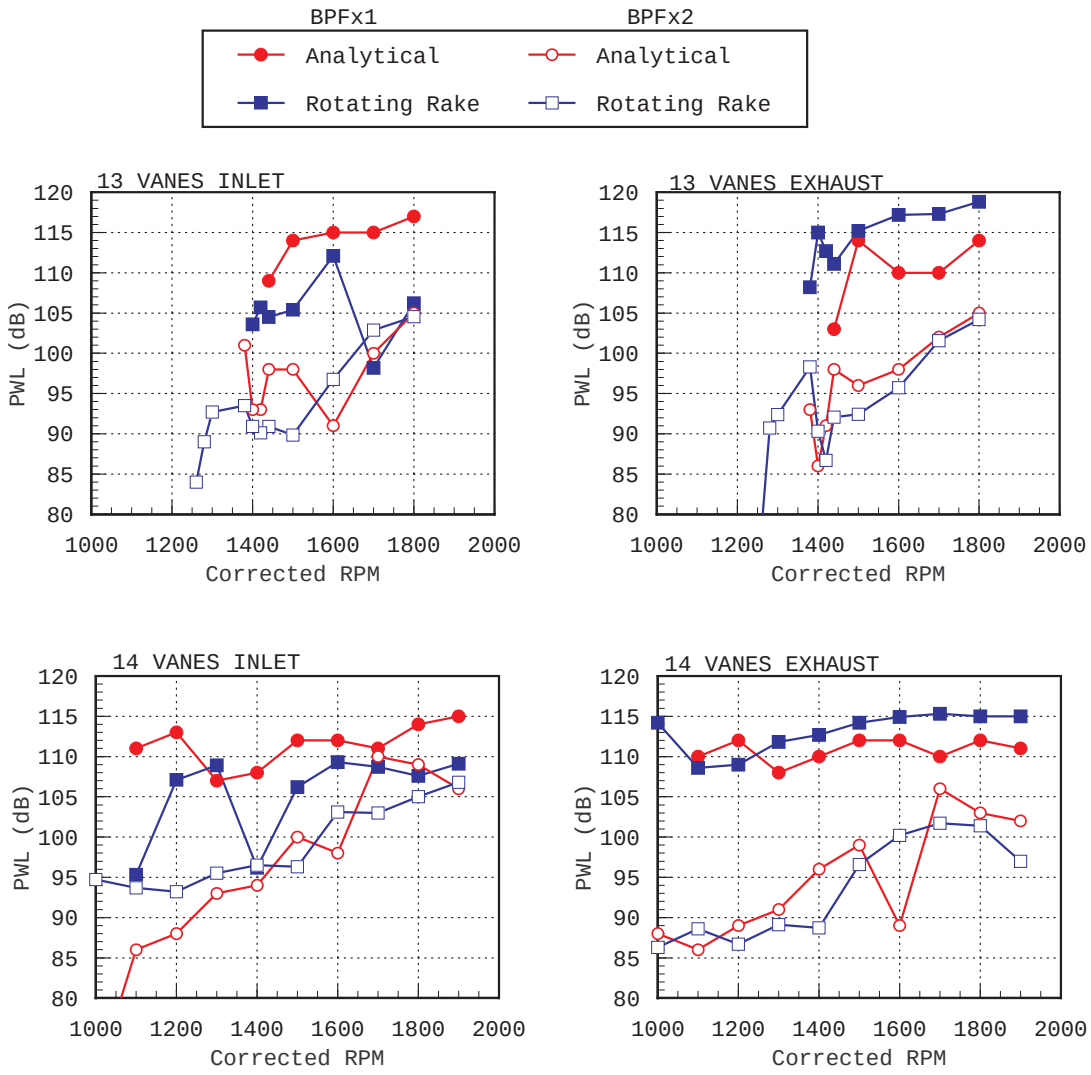

Figure 13a.–Comparison of Analytical to Measured Mode PWL.
(Inlet/Exhaust PWL at BPF & 2BPF)

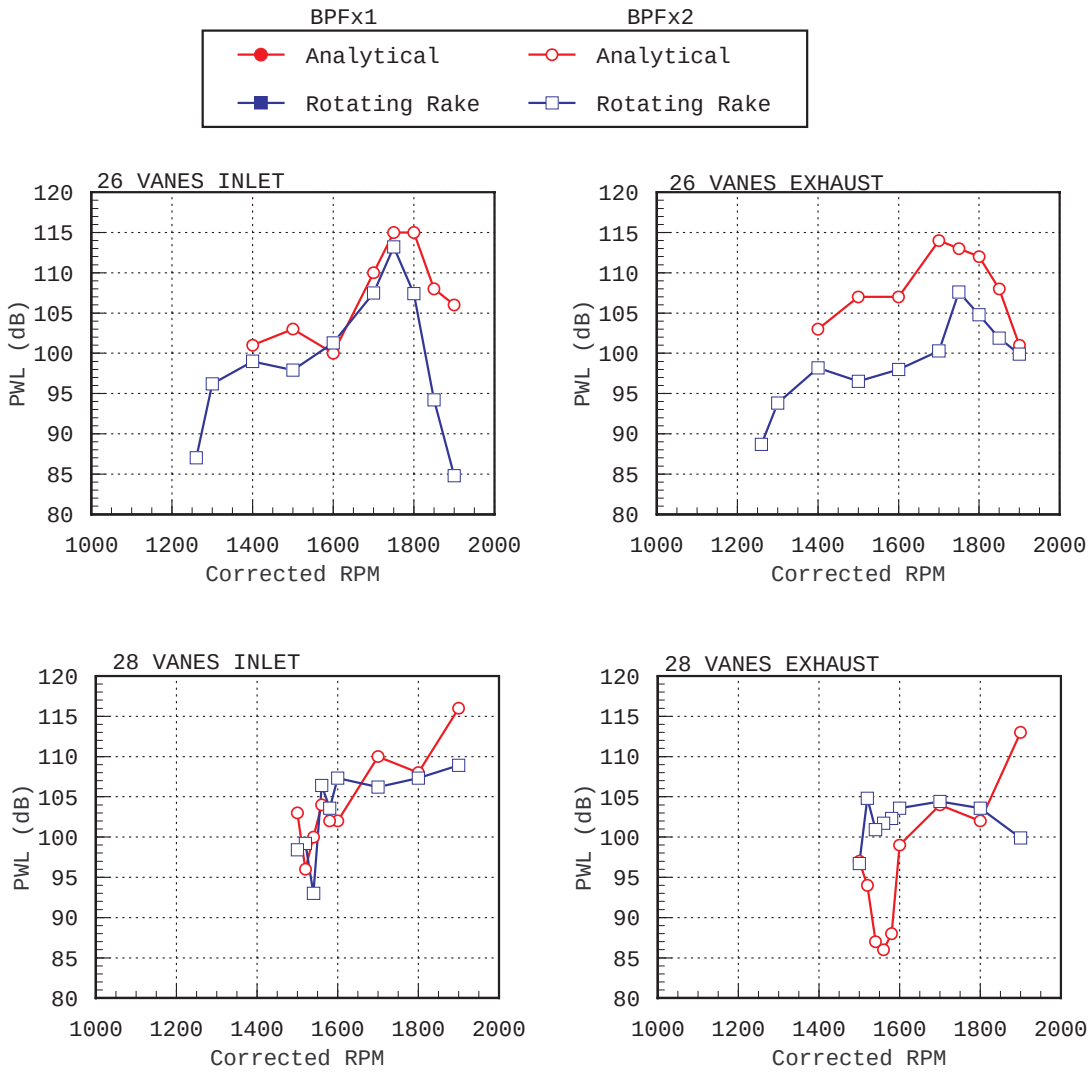

Figure 13b.–Comparison of Analytical to Measured Mode PWL.
(Inlet/Exhaust PWL at 2BPF)

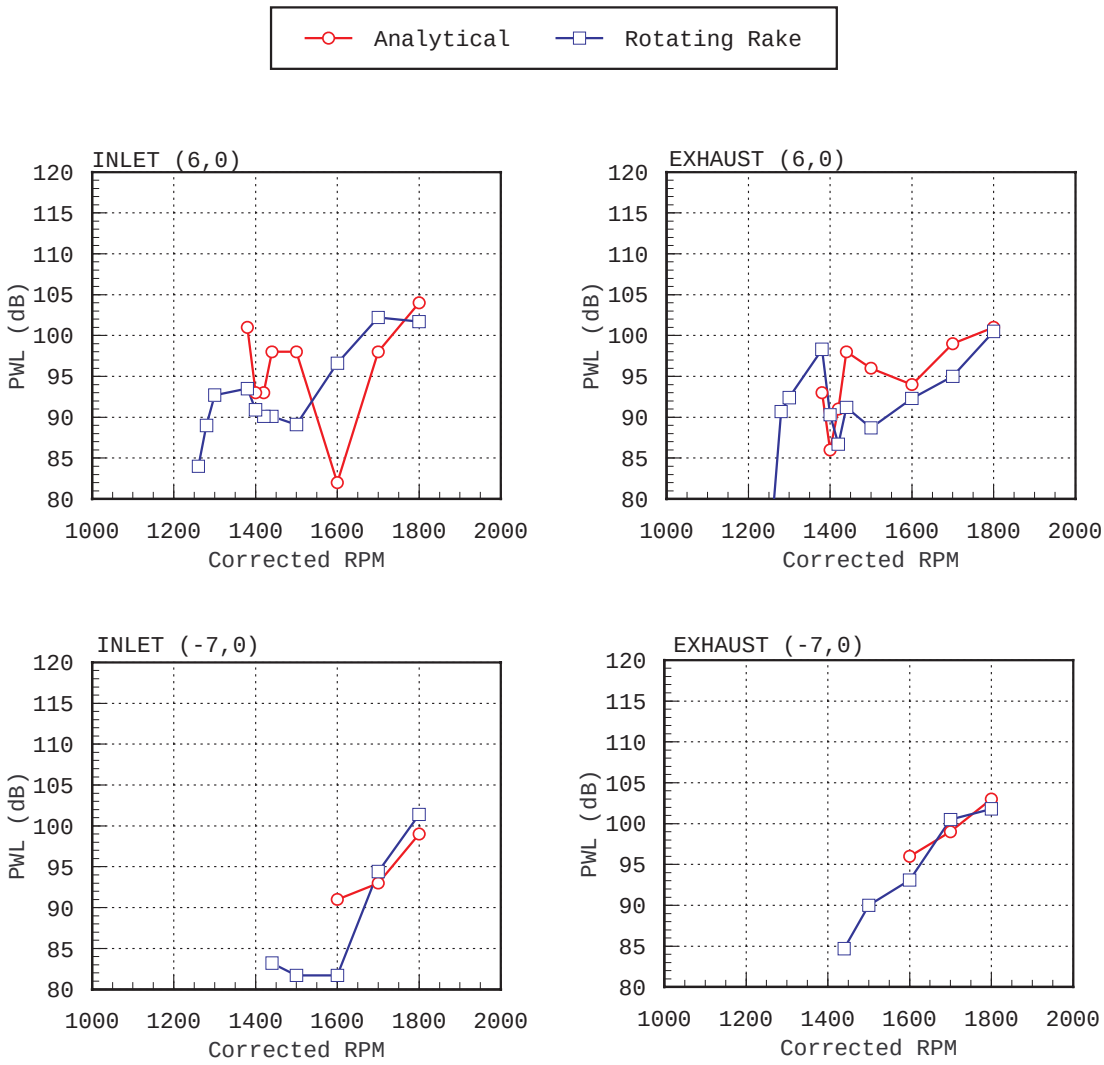

Figure 14a.–Comparision of Analytical to Measured Mode PWL.
(13 Vanes Individual Mode PWL at 2BPF)

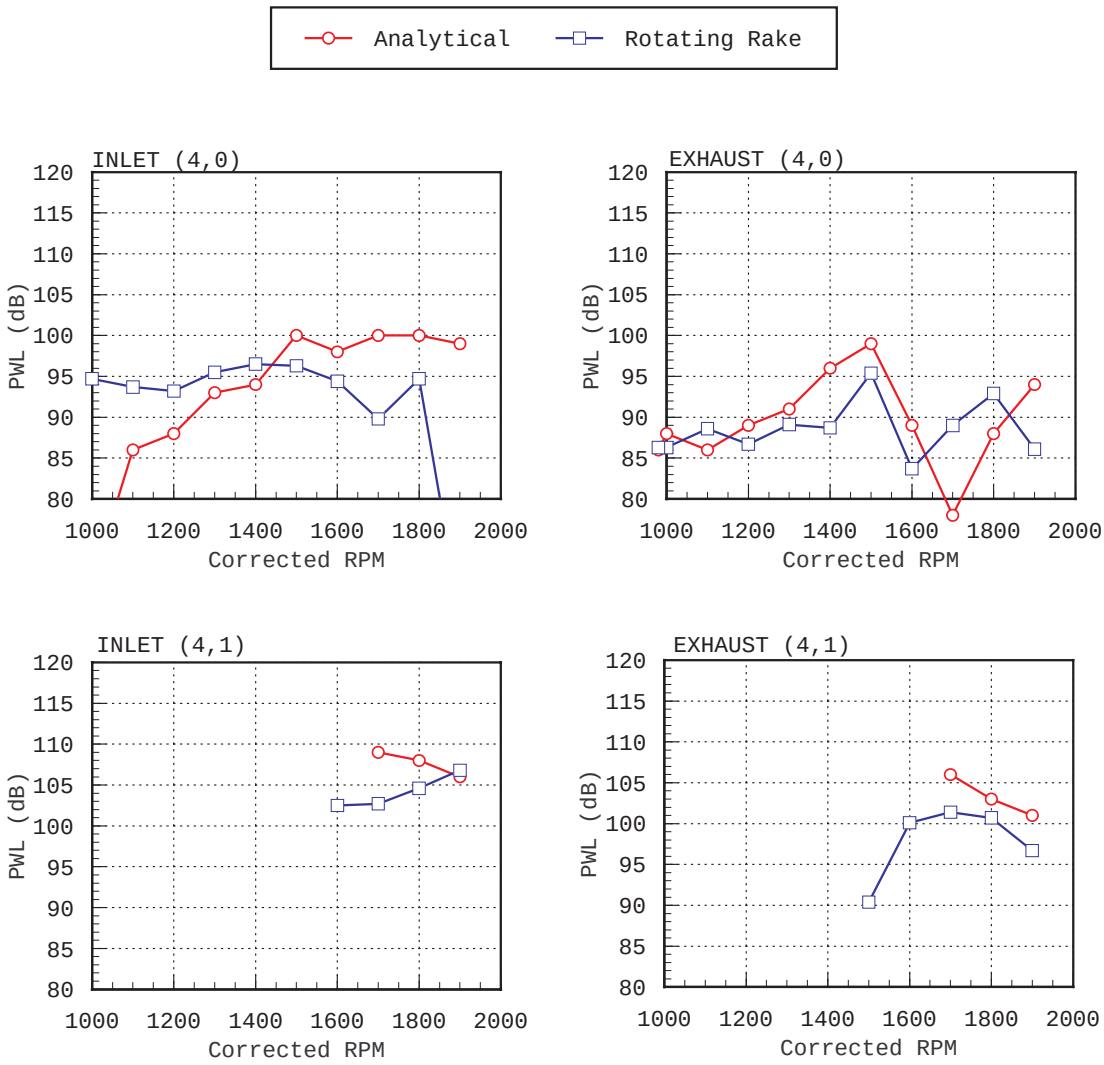

Figure 14b.–Comparison of Analytical to Measured Mode PWL.
(14 Vanes Individual Mode PWL at 2BPF)

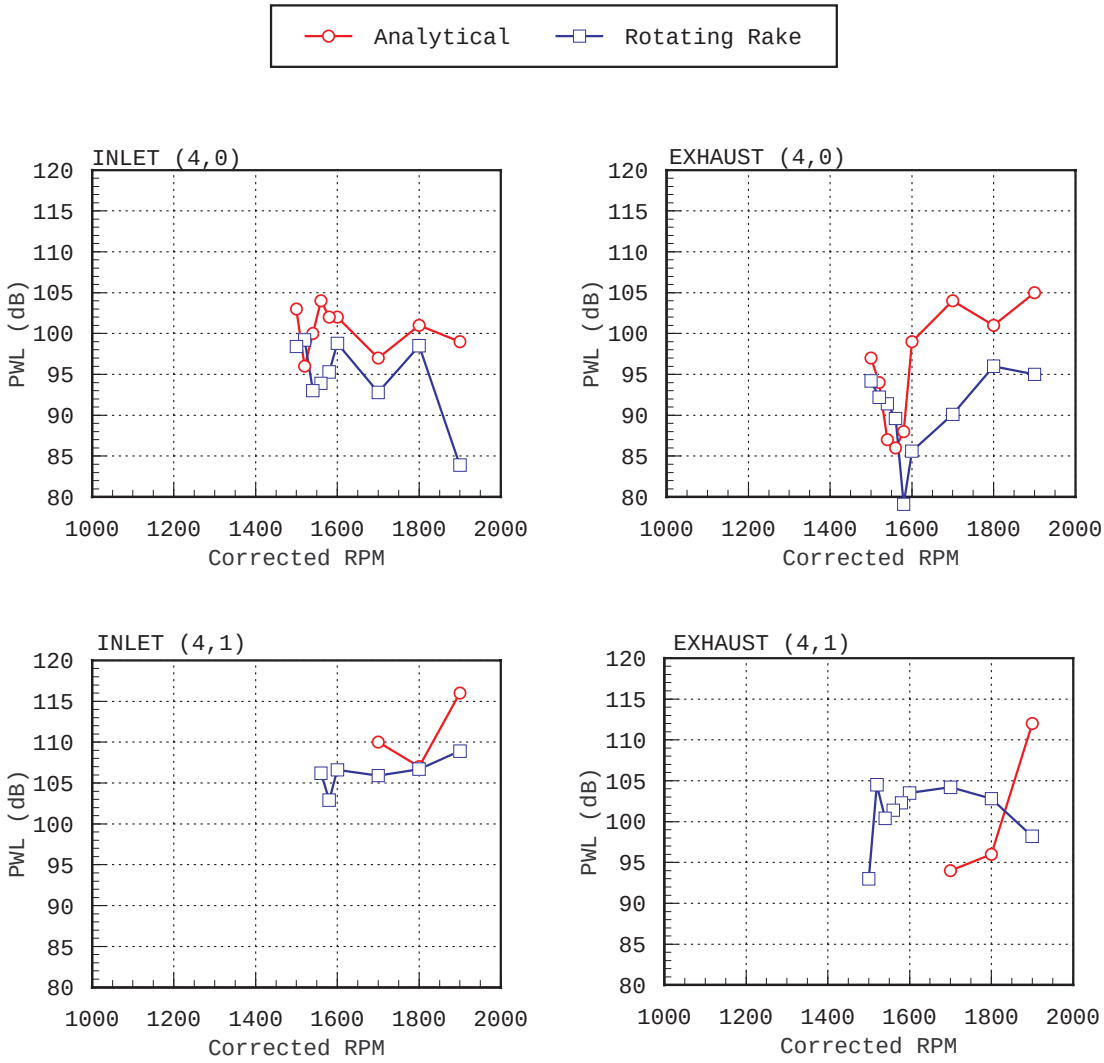

Figure 14c.–Comparison of Analytical to Measured Mode PWL.
(28 Vanes Individual Mode PWL at 2BPF)

APPENDIX

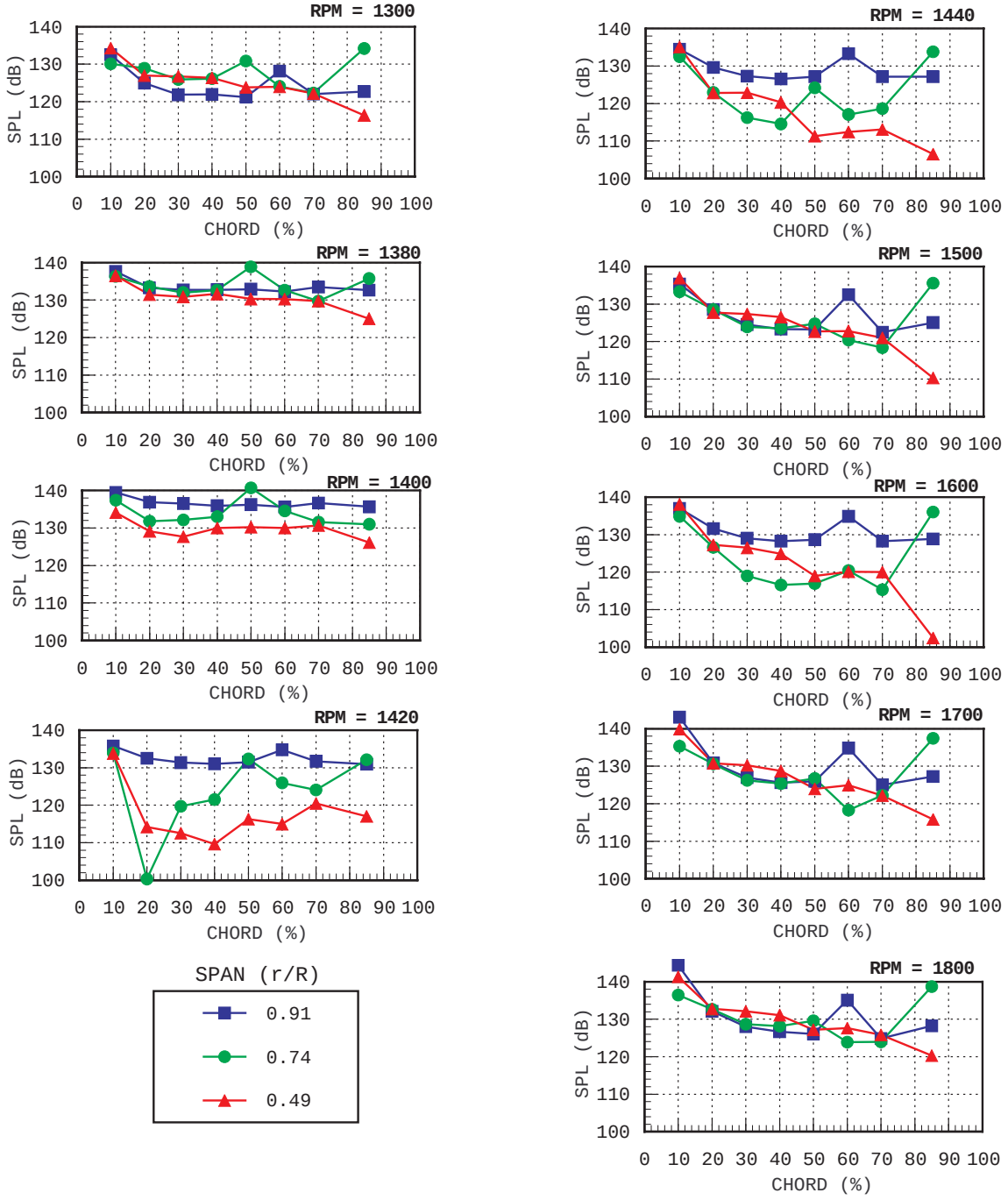

Figure A1.–13 Vanes BPF Magnitude.

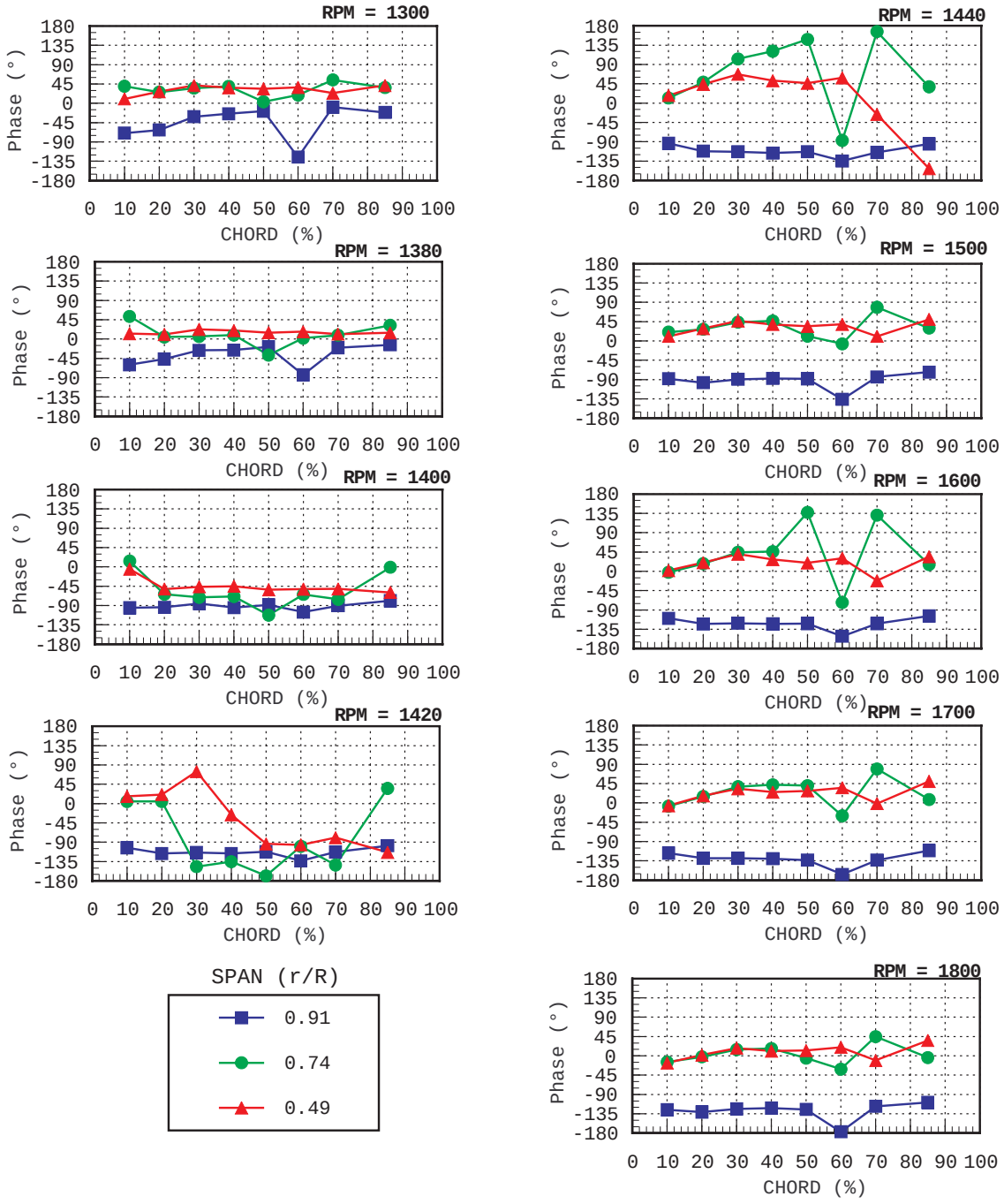

Figure A2.–13 Vanes BPF Phase.

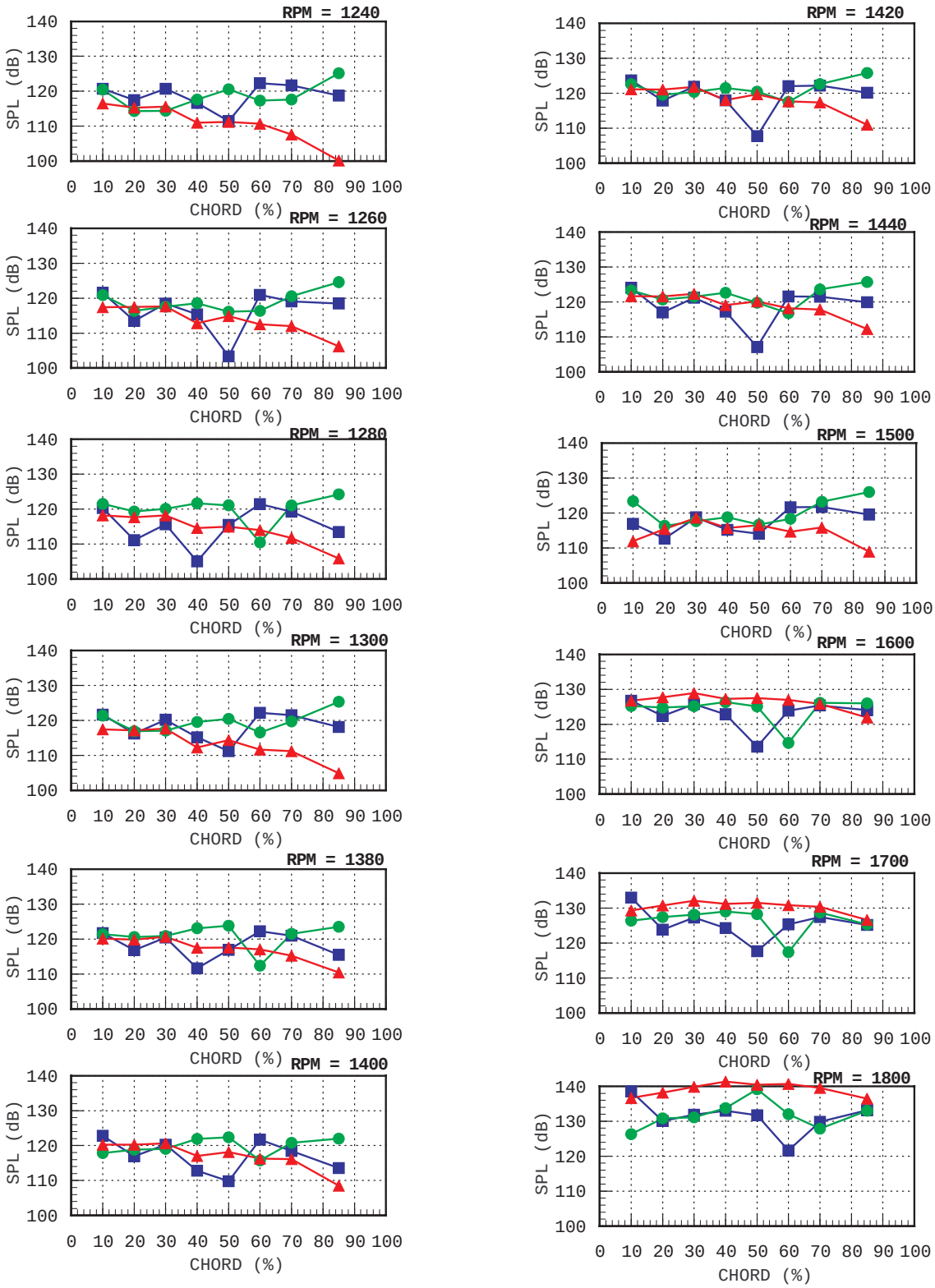

Figure A3.–13 Vanes 2BPF Magnitude.

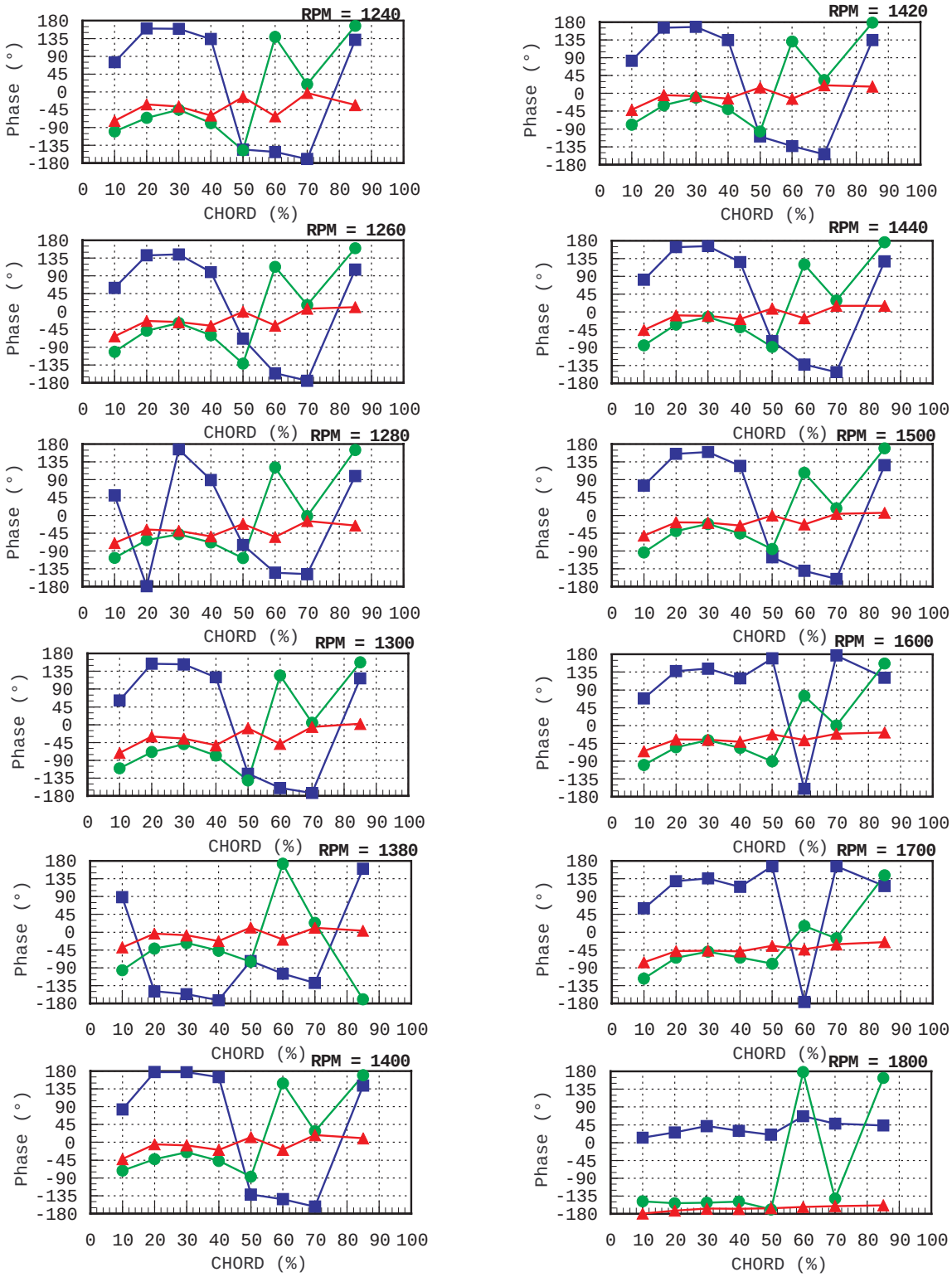

Figure A4.–13 Vanes 2BPF Phase.

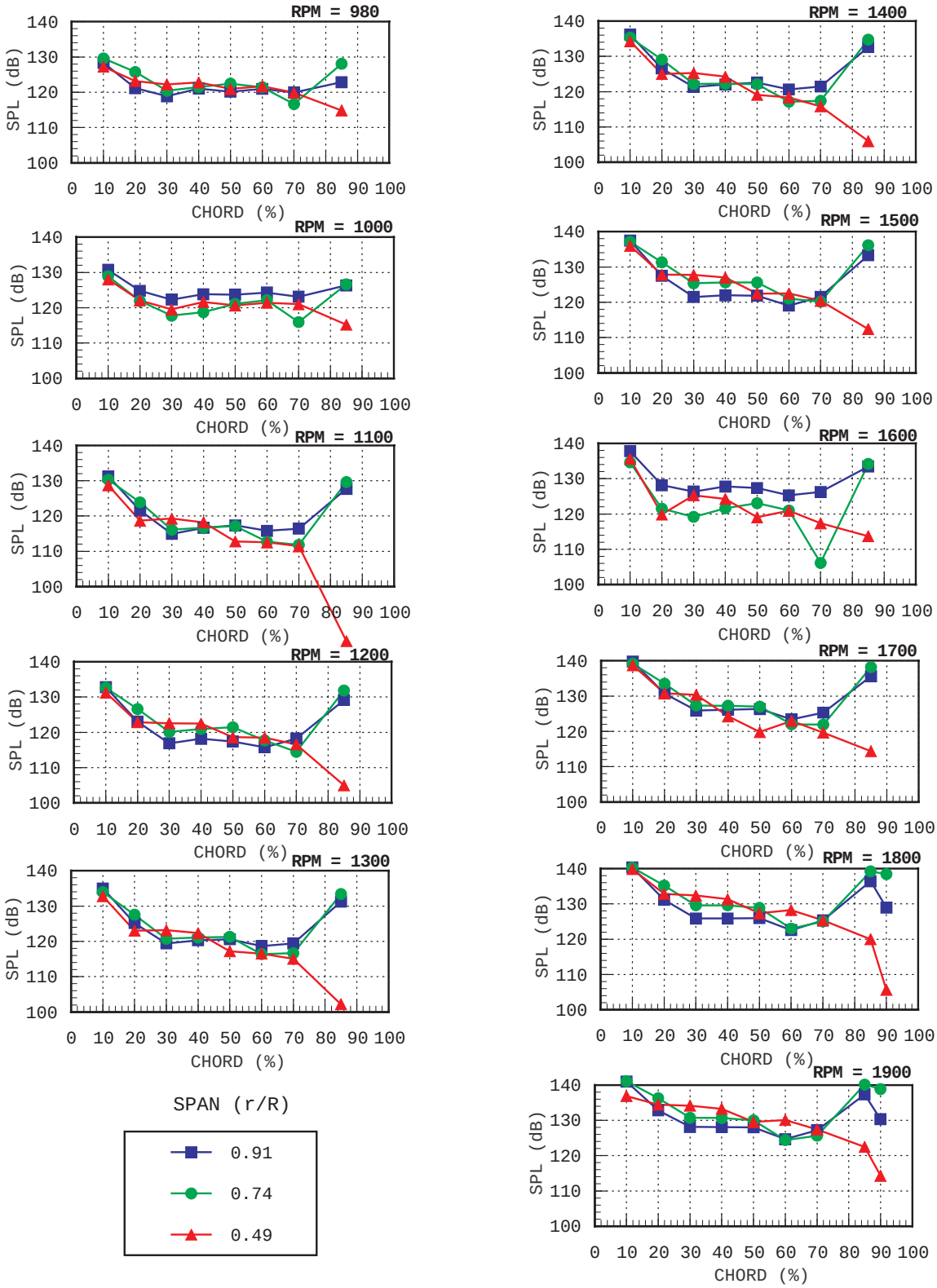

Figure A5.–14 Vanes BPF Magnitude.

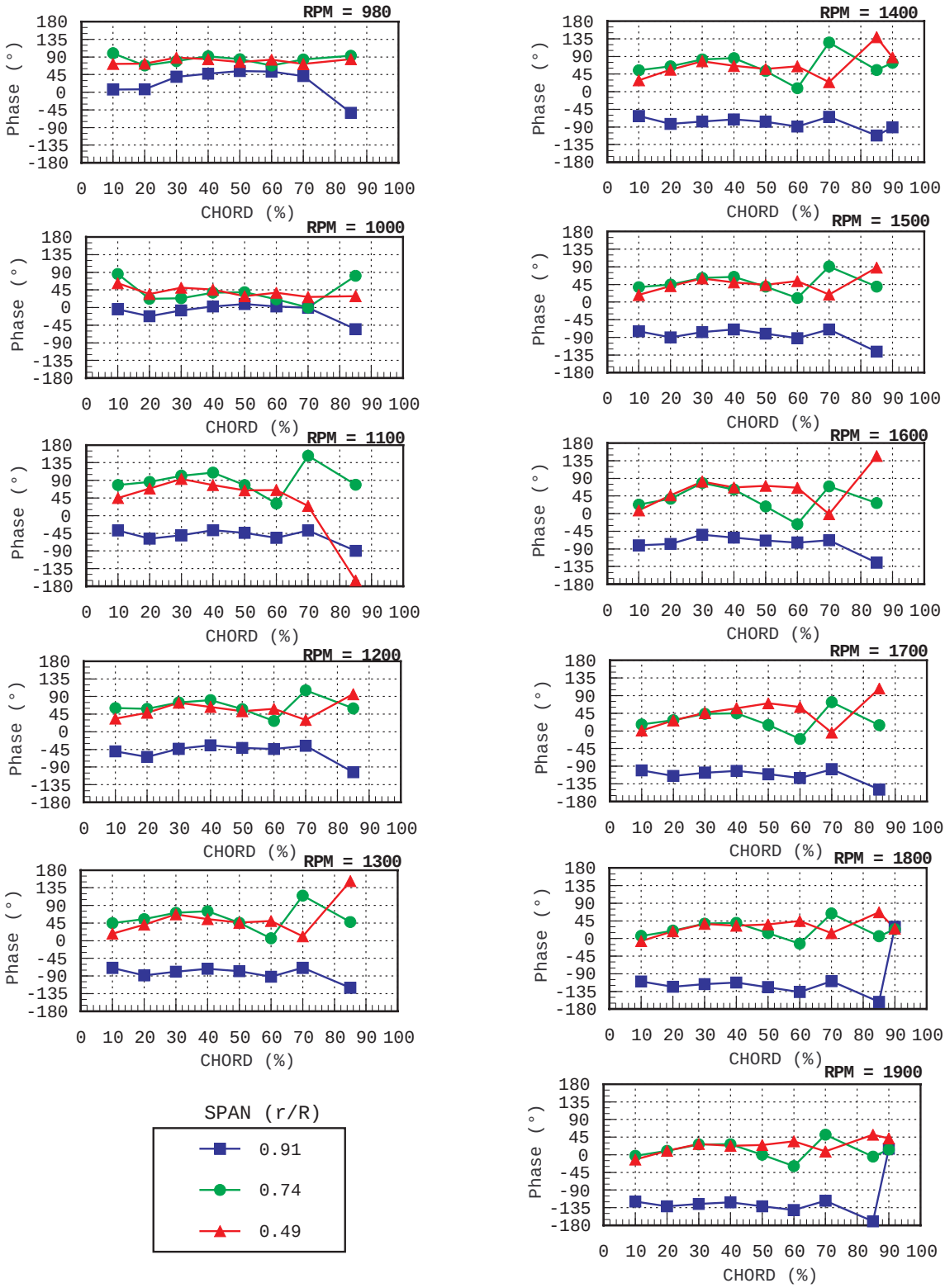

Figure A6.–14 Vanes BPF Phase.

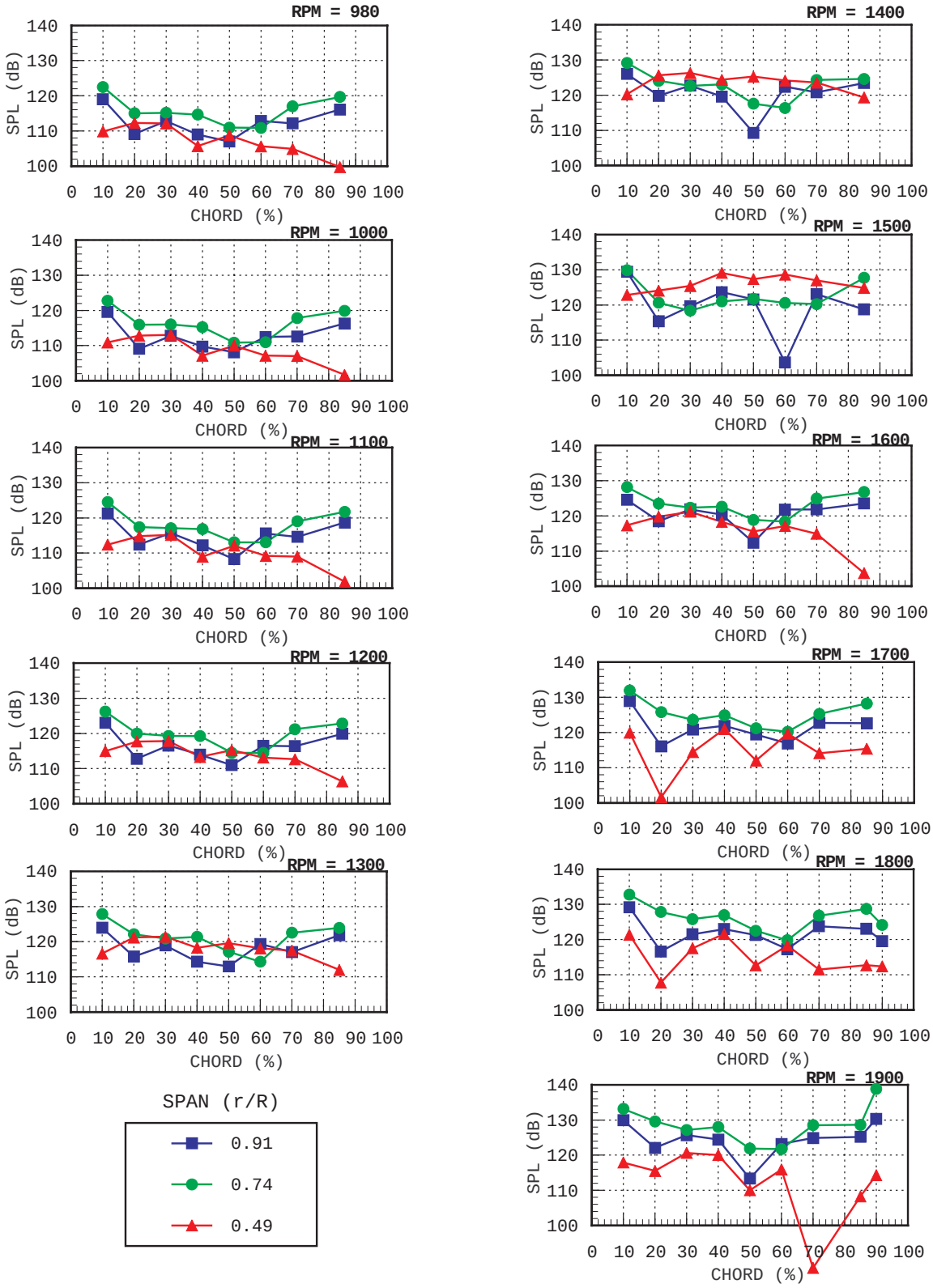

Figure A7.–14 Vanes 2BPF Magnitude.

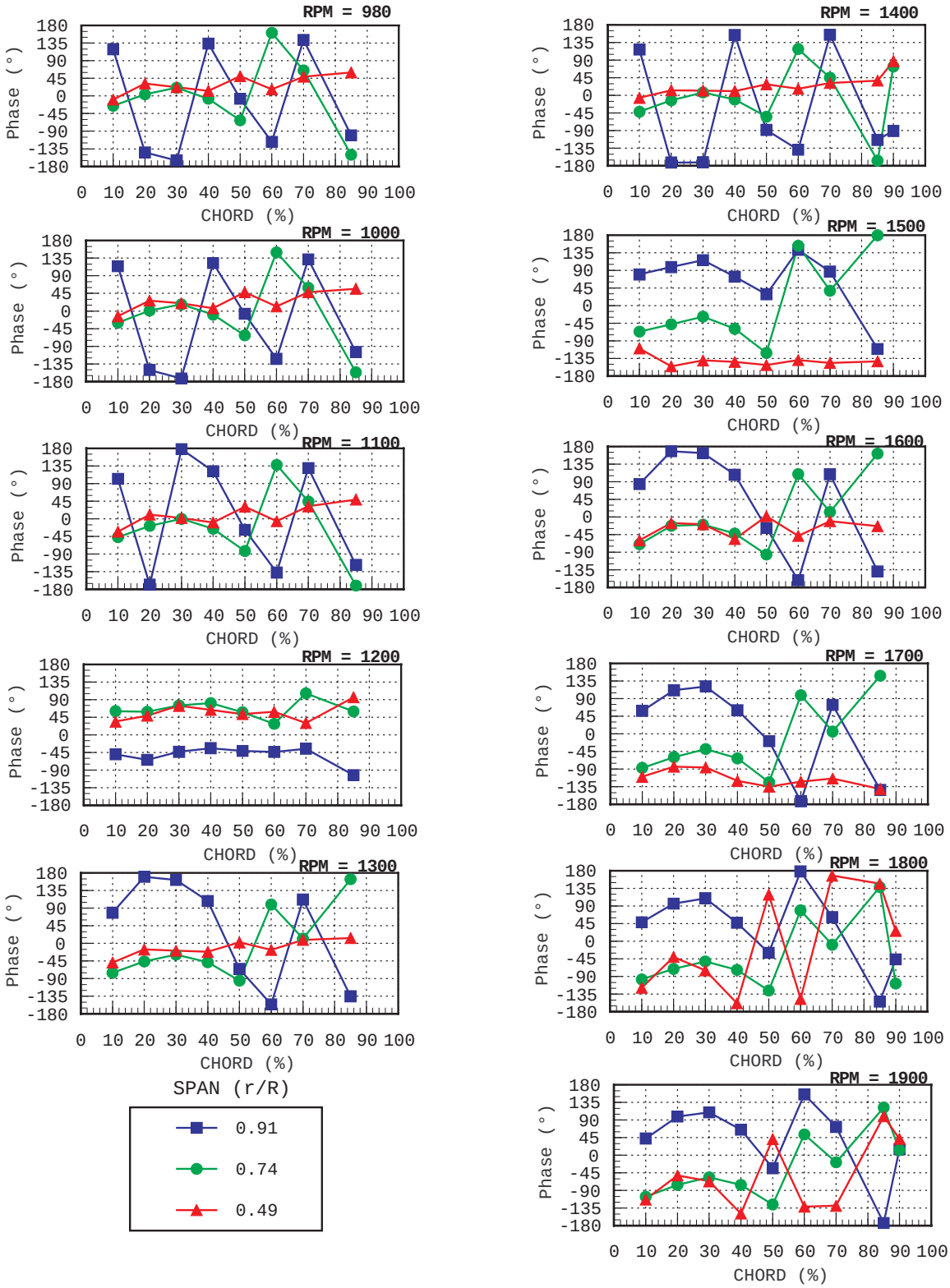

Figure A8.–14 Vanes 2BPF Phase.

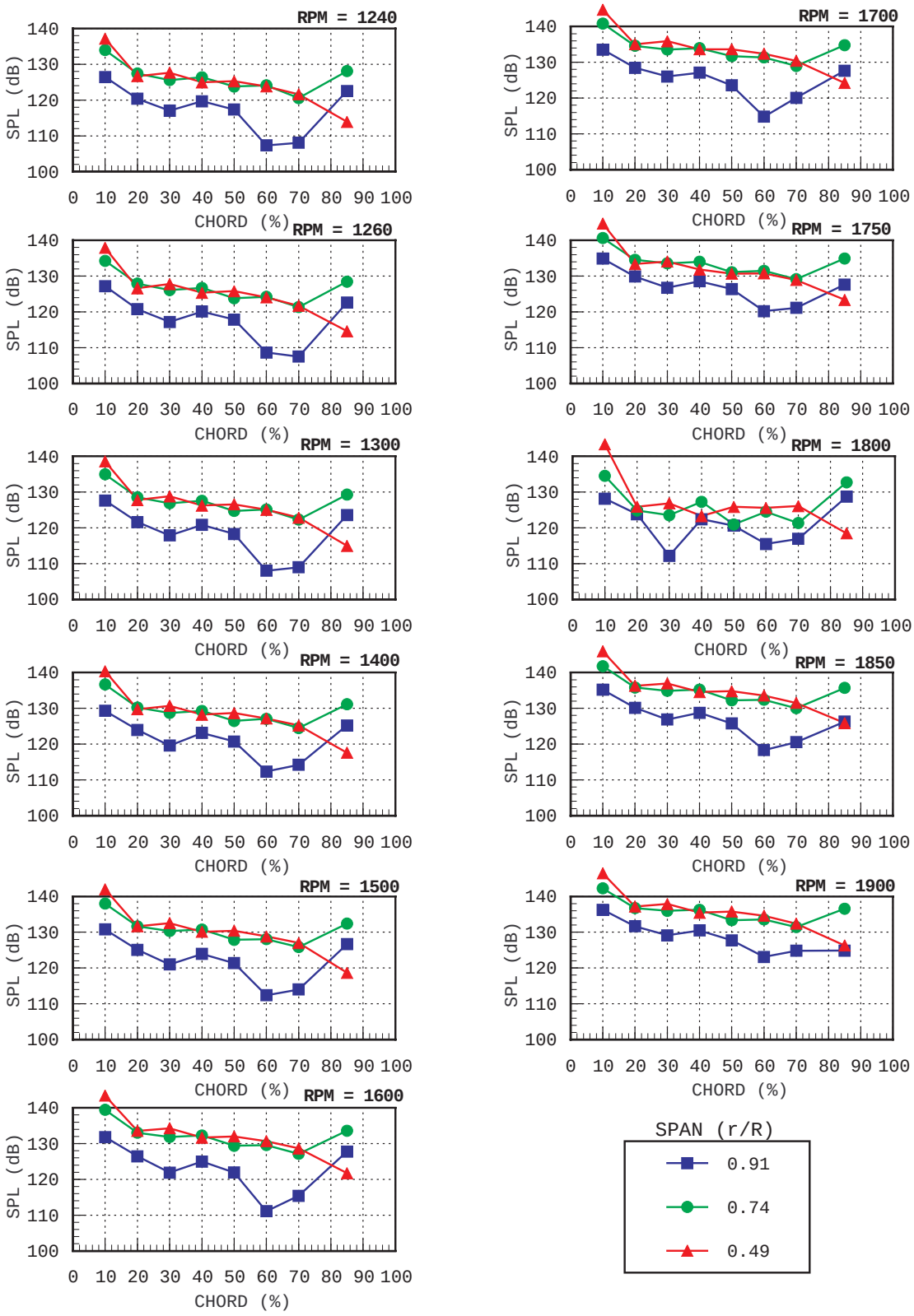

Figure A9.-26 Vanes BPF Magnitude.

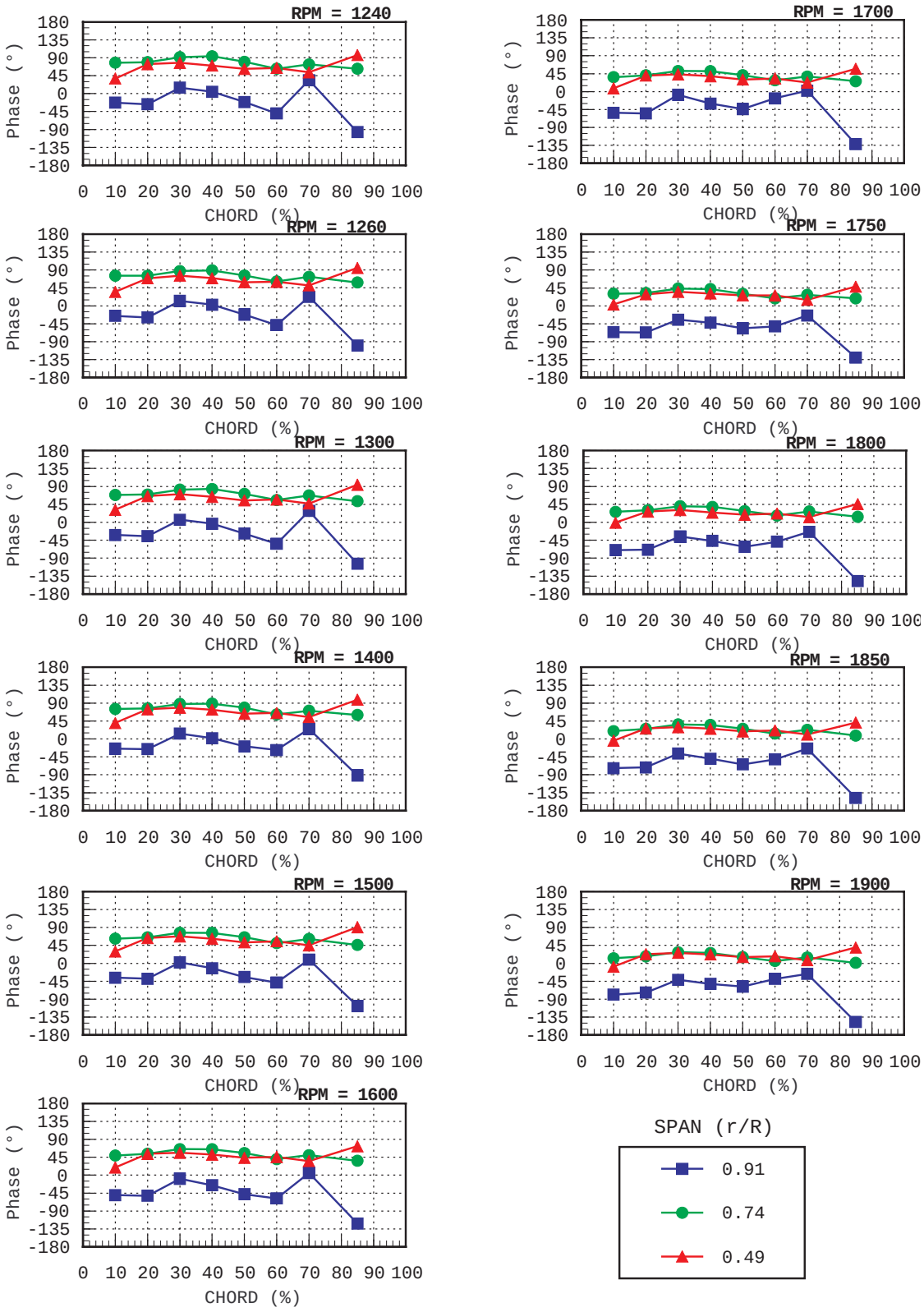

Figure A10.–26 Vanes BPF Phase.

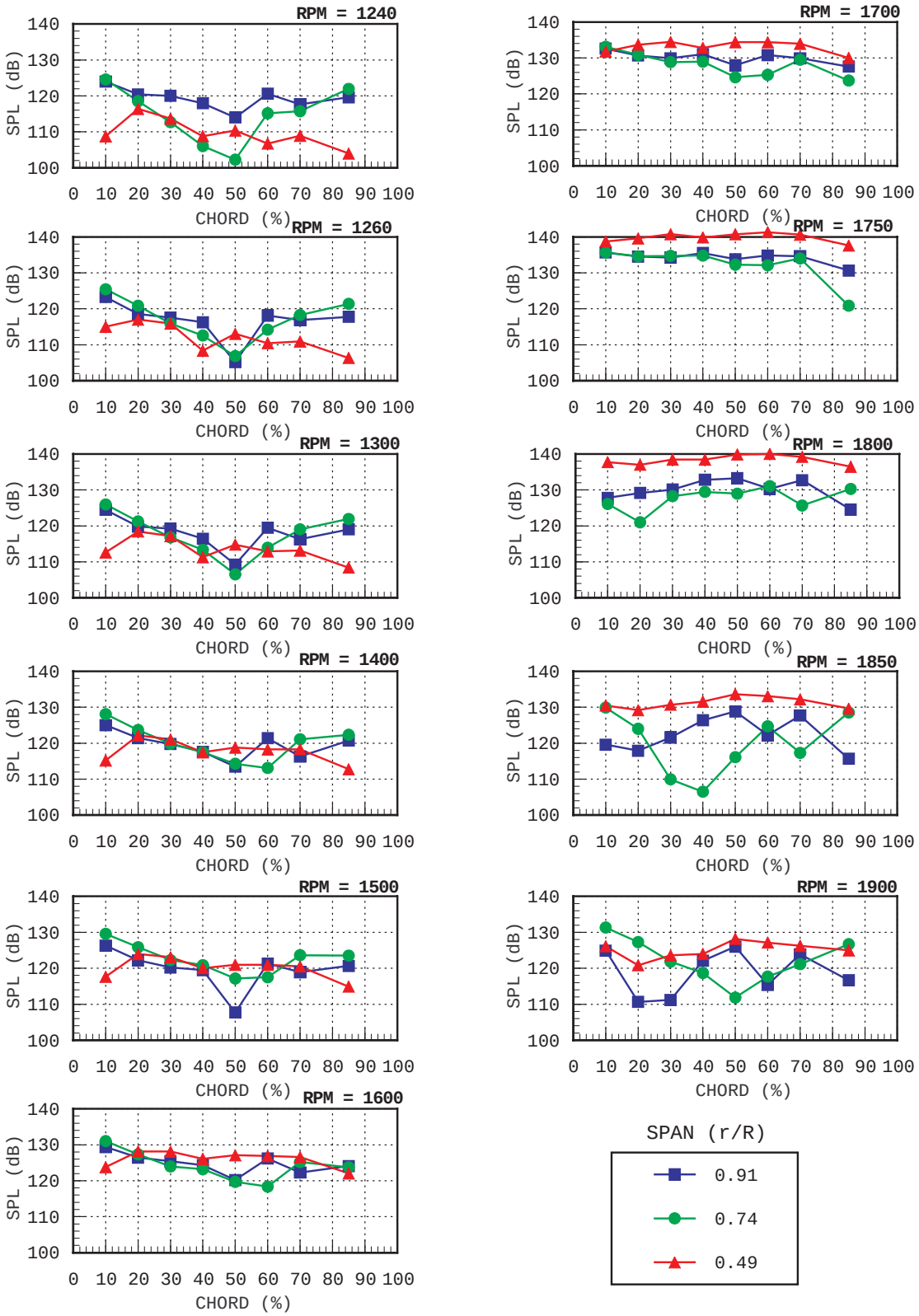

Figure A11.–26 Vanes 2BPF Magnitude.

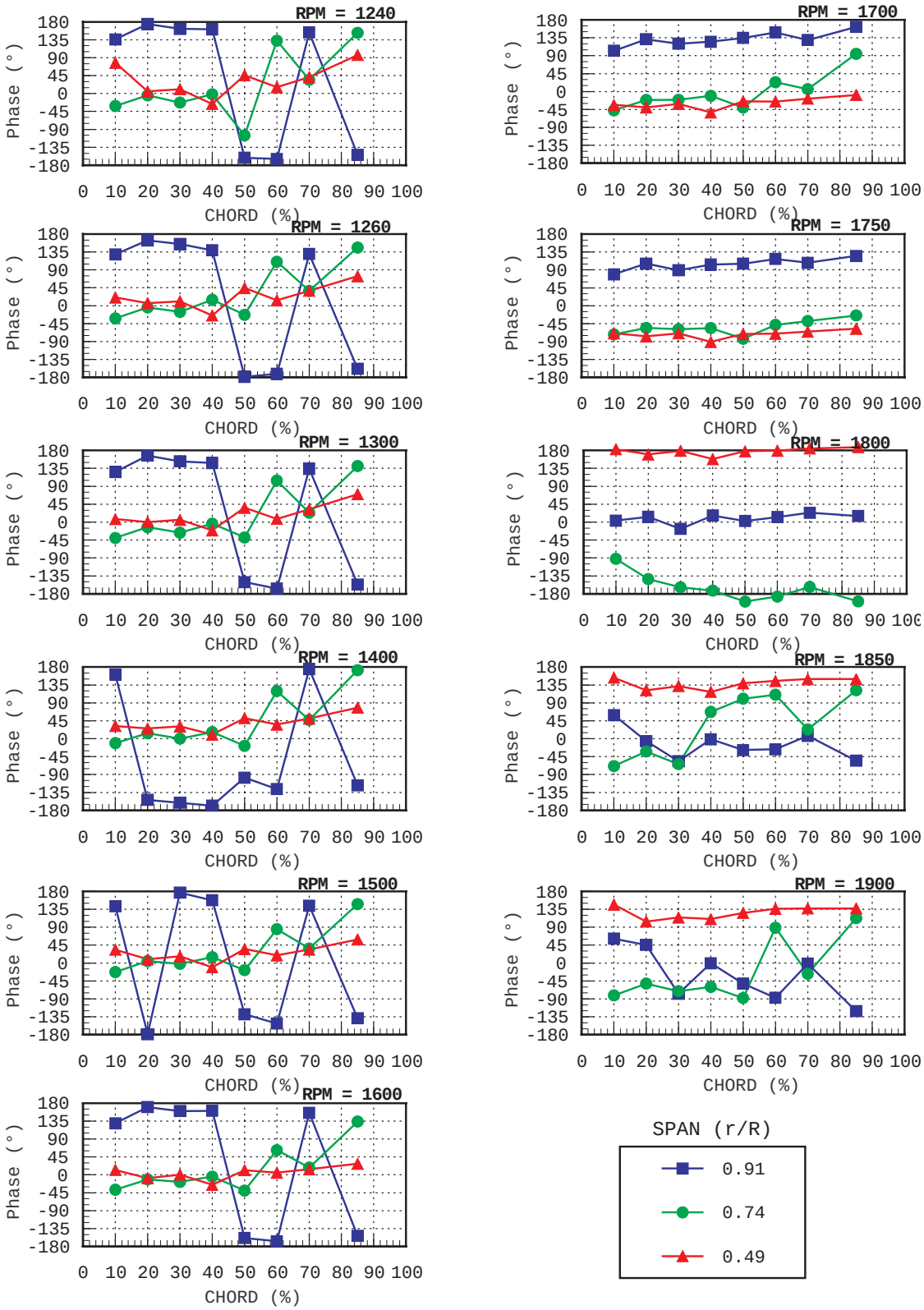

Figure A12.–26 Vanes 2BPF Phase.

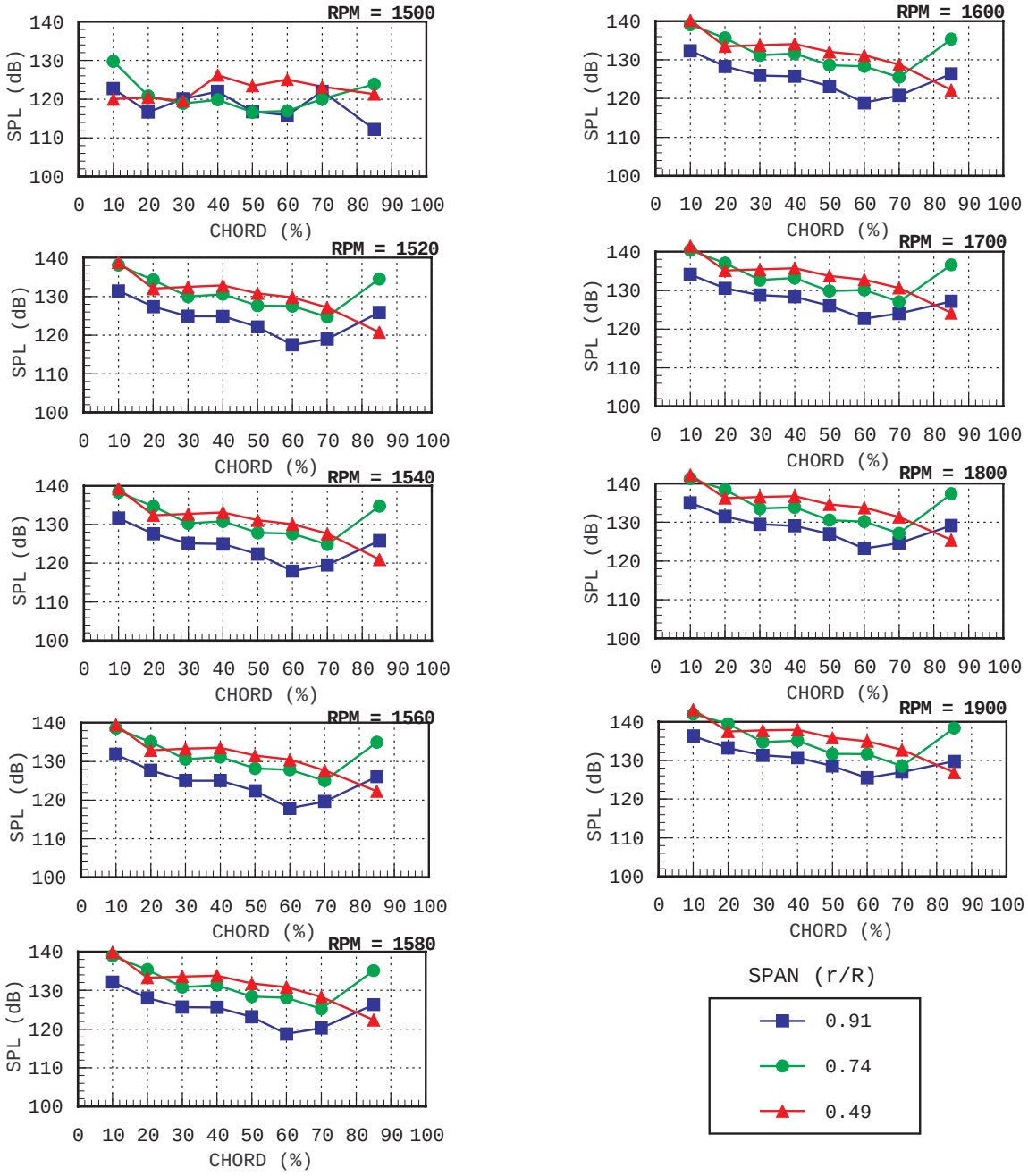

Figure A13.–28 Vanes BPF Magnitude.

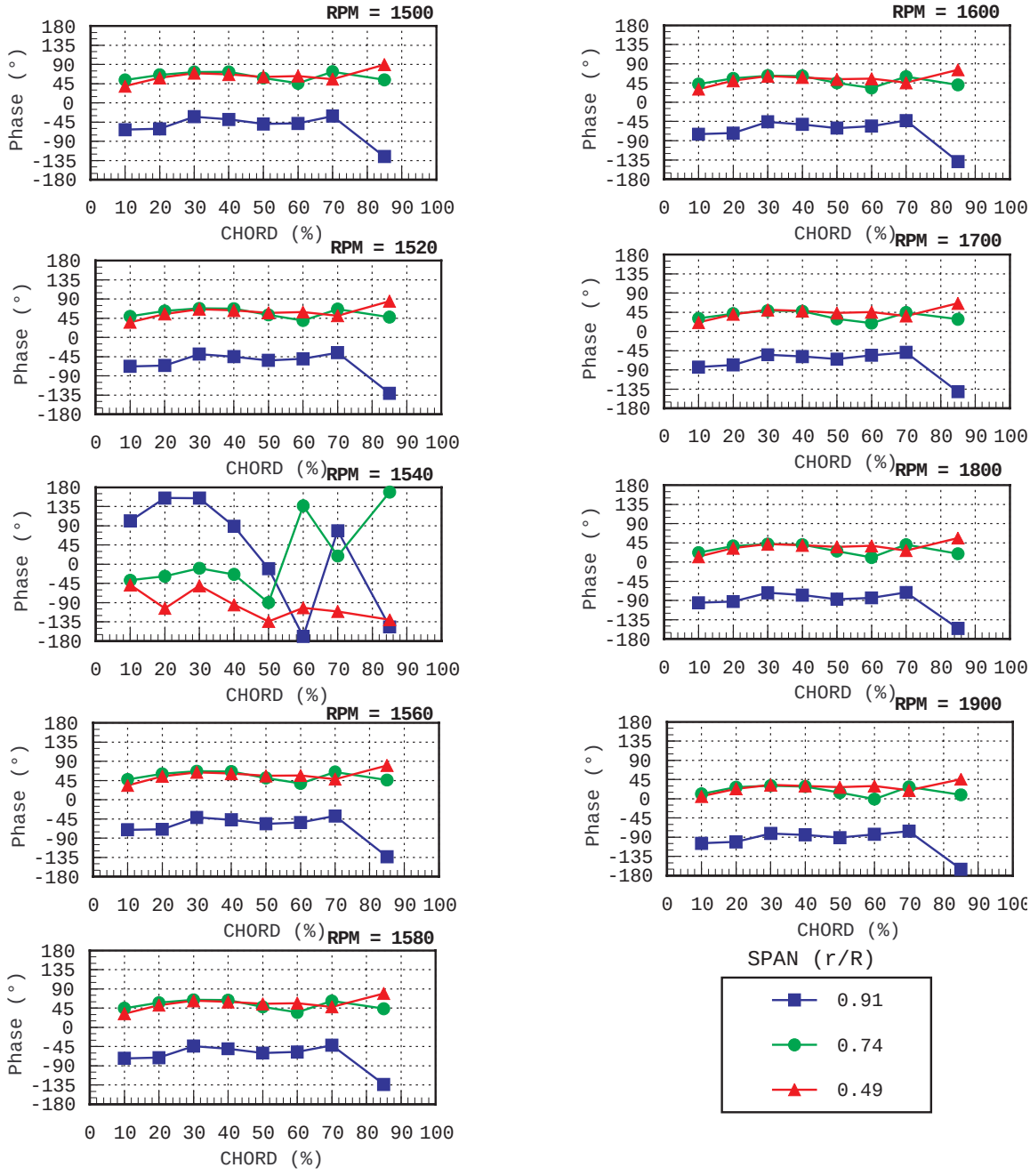

Figure A14.–28 Vanes BPF Phase.

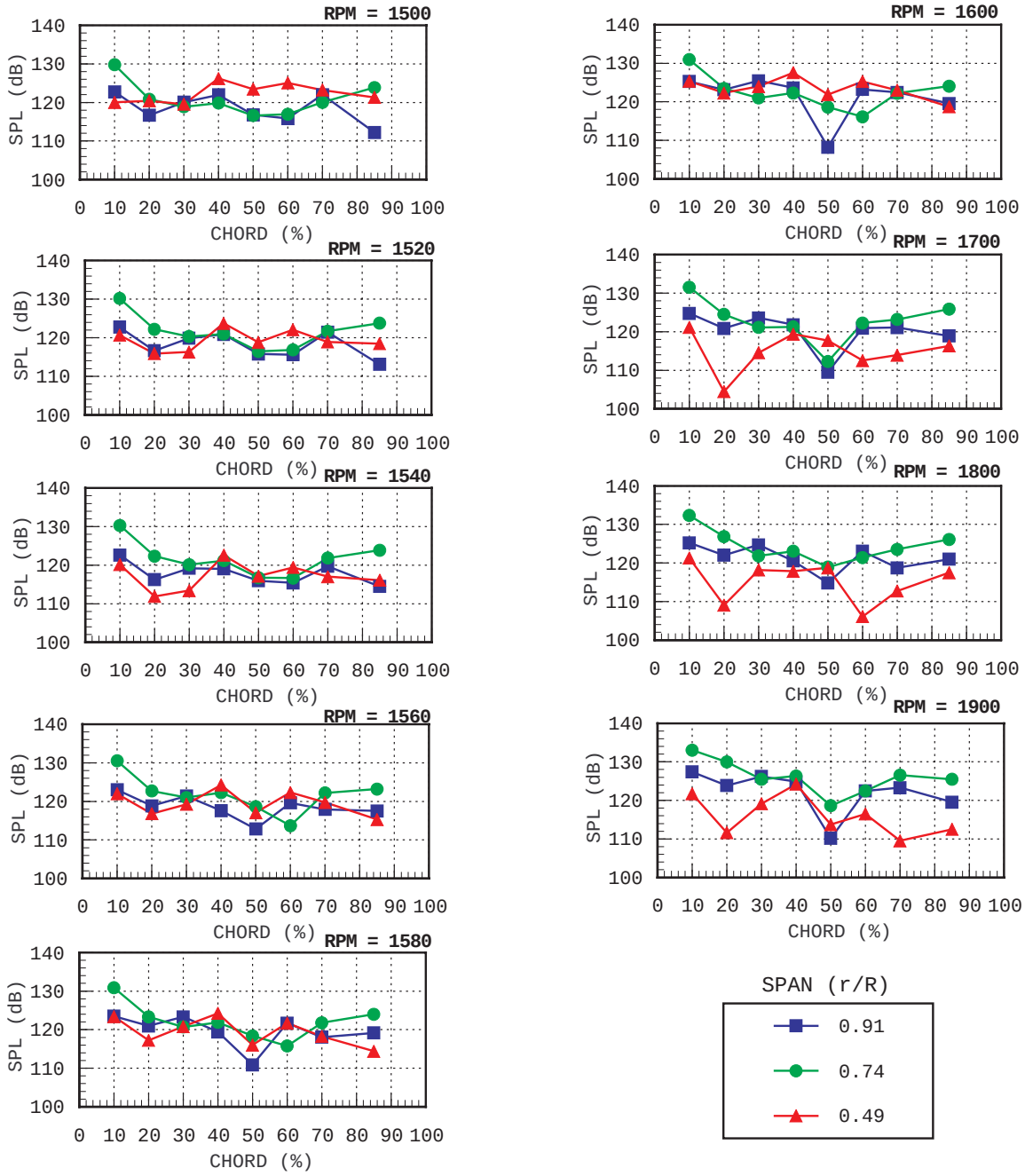

Figure A15.–28 Vanes 2BPF Magnitude.

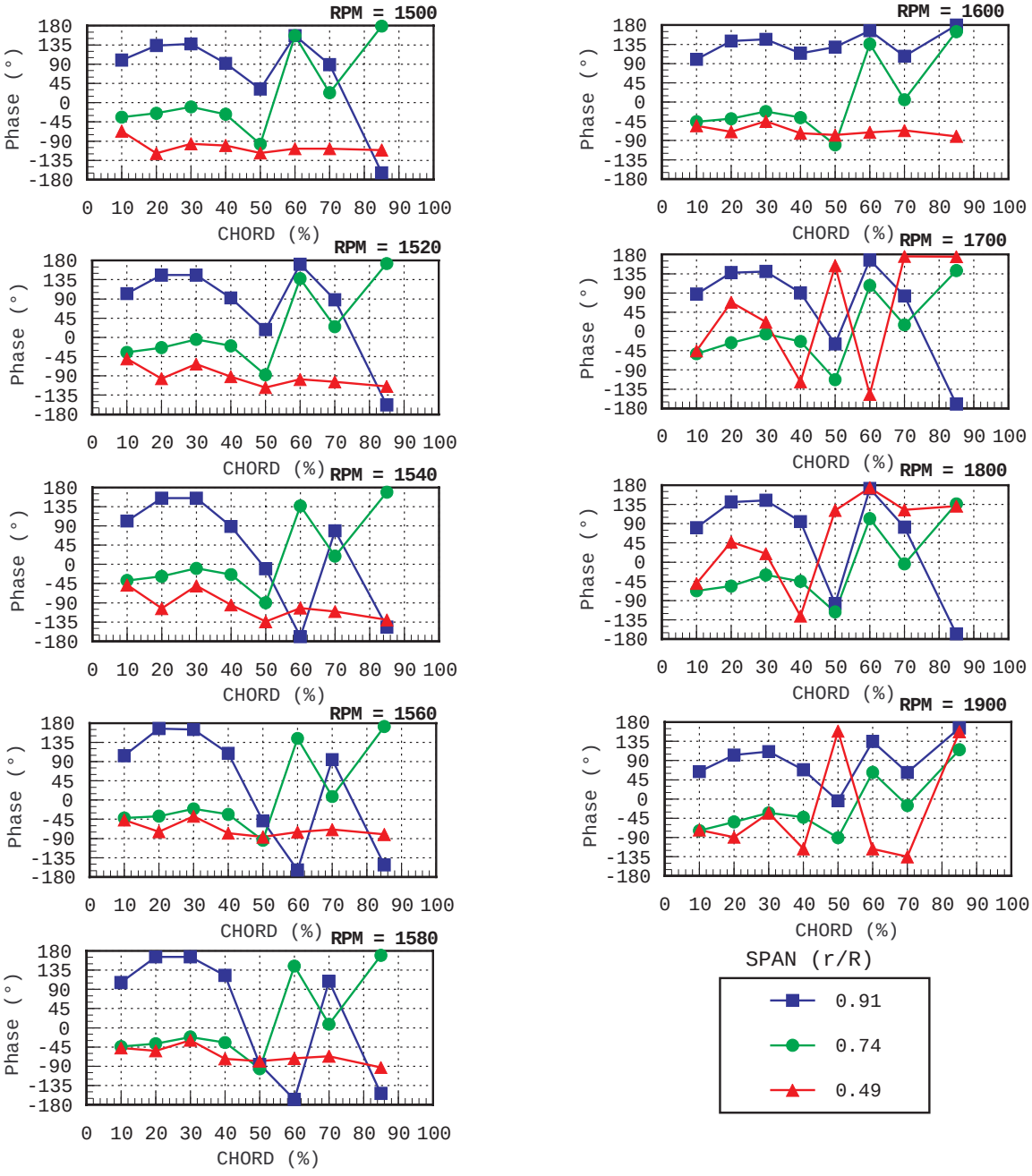

Figure A16.–28 Vanes 2BPF Phase.

REPORT DOCUMENTATION PAGE

Form Approved
OMB No. 0704-0188

1. AGENCY USE ONLY (*Leave blank*)	2. REPORT DATE	3. REPORT TYPE AND DATES COVERED
	May 1999	Technical Memorandum

4. TITLE AND SUBTITLE

Coupling of Low Speed Van Stator Vane Unsteady Pressures to Duct Modes: Measured vs. Predicted

5. FUNDING NUMBERS

WU–538–03–11–00

6. AUTHOR(S)

Daniel L. Sutliff, Laurence J. Heidelberg, and Edmane Envia

7. PERFORMING ORGANIZATION NAME(S) AND ADDRESS(ES)

National Aeronautics and Space Administration
John H. Glenn Research Center at Lewis Field
Cleveland, Ohio 44135–3191

8. PERFORMING ORGANIZATION REPORT NUMBER

E–11583

9. SPONSORING/MONITORING AGENCY NAME(S) AND ADDRESS(ES)

National Aeronautics and Space Administration
Washington, DC 20546–0001

10. SPONSORING/MONITORING AGENCY REPORT NUMBER

NASA TM—1999-209050
AIAA–99–1864

11. SUPPLEMENTARY NOTES

Prepared for the 5th Aeroacoustics Conference sponsored by the American Institute of Aeronautics and Astronautics and the Confederation of European Aerospace Societies, Seattle, Washington, May 10–12, 1999. Daniel L. Sutliff, AYT Corporation, 2001 Aerospace Parkway, Brook Park, Ohio 44142; Laurence J. Heidelberg and Edmane Envia, NASA Glenn Research Center. Responsible person, Daniel L. Sutliff, organization code 5940, (216) 433–6290.

12a. DISTRIBUTION/AVAILABILITY STATEMENT

Unclassified - Unlimited
Subject Categories: 01 and 71 Distribution: Nonstandard

This publication is available from the NASA Center for AeroSpace Information, (301) 621–0390.

12b. DISTRIBUTION CODE

13. ABSTRACT ***(Maximum 200 words)***

Uniform-flow annular-duct Green's functions are the essential elements of the classical acoustic analogy approach to the problem of computing the noise generated by rotor-stator interaction inside the fan duct. This paper investigates the accuracy of this class of Green's functions for predicting the duct noise levels when measured stator vane unsteady surface pressures are used as input to the theoretical formulation. The accuracy of the method is evaluated by comparing the predicted and measured acoustic power levels for the NASA 48" low speed Active Noise Control Fan. The unsteady surface pressures are measured by an array of microphones imbedded in the suction and pressure sides of a single vane, while the duct mode levels are measured using a rotating rake system installed in the inlet and exhaust sections of the fan duct. The predicted levels are computed using properly weighted integrals of measured surface pressure distribution. The data-theory comparisons are generally quite good particularly when the mode cut-off criterion is carefully interpreted. This suggests that, at least for low speed fans, the uniform-flow annular-duct Green's function theory can be reliably used for prediction of duct mode levels if the cascade surface pressure distribution is accurately known.

14. SUBJECT TERMS	15. NUMBER OF PAGES
Ducted fans; Engine noise; Aeroacoustics; Acoustic modes; Unsteady aerodynamics	47
	16. PRICE CODE
	A03

17. SECURITY CLASSIFICATION OF REPORT	18. SECURITY CLASSIFICATION OF THIS PAGE	19. SECURITY CLASSIFICATION OF ABSTRACT	20. LIMITATION OF ABSTRACT
Unclassified	Unclassified	Unclassified	